Ingineria automobilului

Registrul Auto Român

SIAR

Societatea Inginerilor de Automobile din România

SE DISTRIBUIE GRATUIT CA SUPLIMENT AL REVISTEI AUTOTEST
ISSN 1842 – 4074
Nr. 67 / iunie 2023

SIAR – KLC 2023

Challenge Kart Low Cost – Ediția a XI-a
16-17 mai 2023

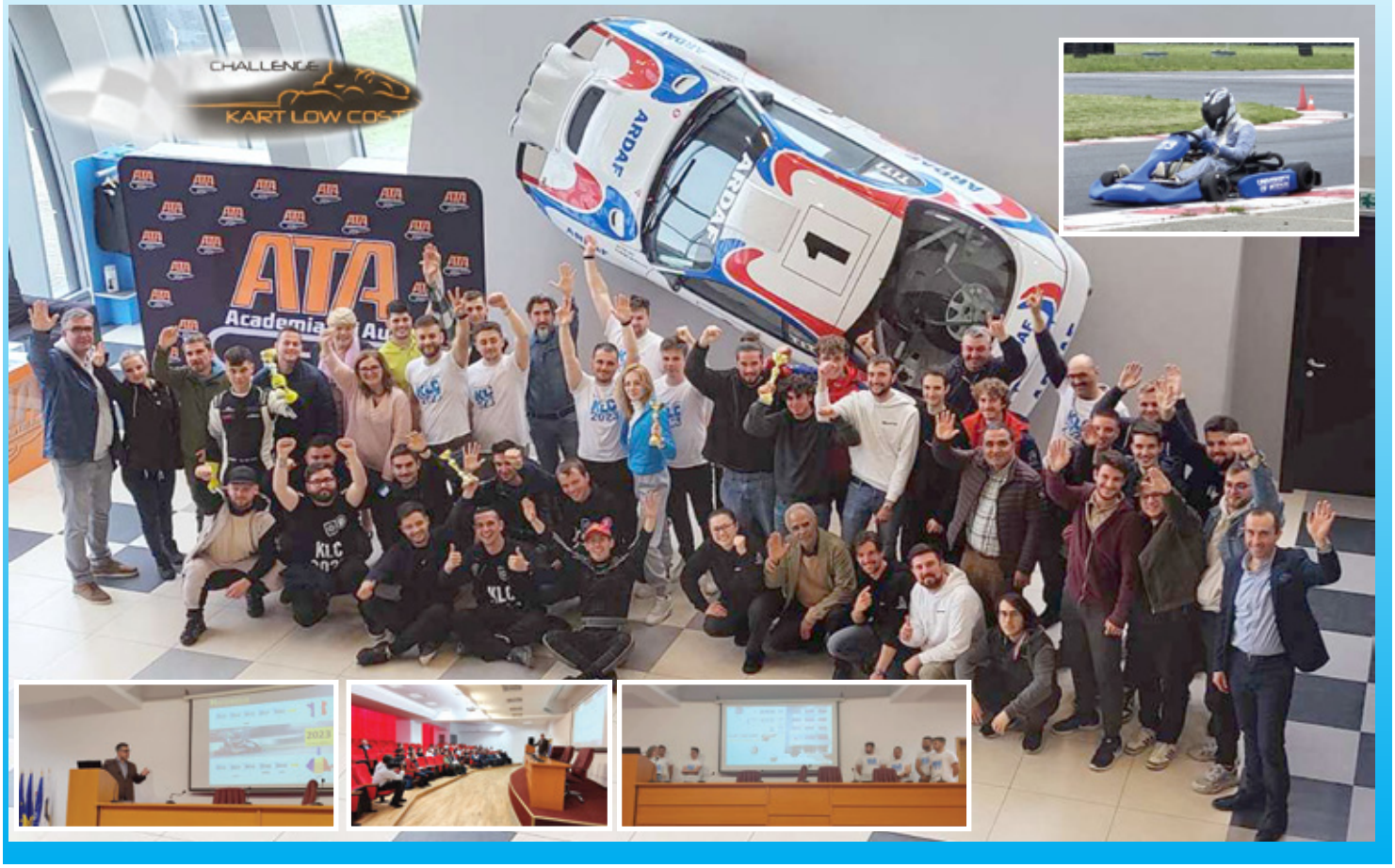

- Raport de comprimare versus raport de destindere
- Analiza unei bielete de direcție în prezența incertitudinilor parametrice
- Studiul influenței parasolarului asupra câmpului vizual al șoferului utilizând sisteme de simulare a realității virtuale
- KLC 2023
- In memoriam: Prof. univ. dr. ing. Eugen-Mihai Negruș

SIAR ESTE MEMBRĂ FISITA INTERNATIONAL FEDERATION OF AUTOMOTIVE ENGINEERING SOCIETIES
EAEC EUROPEAN AUTOMOBILE ENGINEERS COOPERATION
APARE TRIMESTRIAL QUARTERLY

The 33rd SIAR International Automotive and Transportation Engineering Congress

ESFA 2023

2 – 4 November 2023, Bucharest, Romania

Congress Subject: *„Fuel Economy, Safety and Reliability of Motor Vehicles"*

Congress Topics:

1. *Smart Vehicles*
2. *Green Vehicles (HEV and EV)*
3. *Advanced Powertrains (engine and transmission)*
4. *Advanced Engineering Methods and Tools*
5. *Fuel Economy and Pollution Control*
6. *New Materials and Technologies*
7. *Vehicles Dynamics, Safety and Comfort*
8. *Vehicles Design and Testing*
9. *Terrain Vehicles*
10. *Automotive Reliability and Maintenance*
11. *Traffic and Road Transport Systems*
12. *Intelligent Transport Systems*

The 33rd edition of the **International Congress of SIAR of Automotive and Transportation Engineering** is at the same time the 10th **„Fuel Economy, Safety and Reliability of Motor Vehicles")** **Congress** (ESFA – *Economicitatea, Securitatea și Fiabilitatea Autovehiculelor* - in Romanian) **organized by SIAR and hosted from the Politehnica University of Bucharest.**

„Politehnica" University of Bucharest is the most important technical university in Romania. It was founded on March 24, 1818, as school of civil engineers. Starting with 1887 under the name of School of Mines, Bridges and Roads it got a new development. Reorganized in 1930 into Polytechnic Institute of Bucharest it gathered seven faculties: Civil Engineering, Electro-mechanics, Metallurgy, Industrial Chemistry, Forestry, Agronomy and Architecture.

Another important transformation took place in 1948 when several faculties became independent as institutes.

Starting with 1992, it became "POLITEHNICA" University of Bucharest.

With more than 200 years of existence, „Politehnica" University of Bucharest represents one of the fundamental and prestigious institutions representing a guaranty of value and technical competence.

The congress will be accompanied by many events for the participants: exhibition of products specific to the automotive industry, car components and transports, workshops, technical visits, the general meeting of SIAR, the final stage of the international contest for the students on automotive engineering "Professor Eng. Constantin GHIULAI" with the two sections: „Automotive Dynamics" - the 9th edition and „Automotive CAD - CATIA V5" - the 6th edition.

For more information about this event, please visit ***www.siarcongress.eu.***

POSIBILE REVENIRI
POSSIBLE RETURNS

O întâlnire, o discuție și un schimb de opinii m-au determinat să reiau un subiect pe care l-am atins într-o anumită măsură într-un editorial anterior. Se pare că evoluțiile politico-economice-militare din vecinătatea noastră (în care suntem parte într-o anumită măsură) redefinesc priorități pentru statele membre ale Uniunii Europene - și ca atare și pentru țara noastră! Sunt solicitate acțiuni ferme de asigurare a unor echipamente tehnice competitive, numeroase din domeniul nostru de competență (mă refer la autovehicule cu utilizare militară). Și întrebarea legitimă ar fi: sunt posibile acțiuni de reconstituire a capabilităților tehnice și tehnologice românești care să permită realizarea intereselor naționale specifice, în cel mai scurt timp? Altfel spus, ar putea reveni la un nivel acceptabil de „funcționare" industria românească de autovehicule de interes național (asta însemnând pe lângă autocamioane și autospeciale, și autovehicule cu destinație militară: tancuri, mașini de luptă, transportoare blindate, autovehicule blindate ușoare etc.!). Sau altfel spus, industria românească de autovehicule (altele decât autoturisme) ar putea renaște?

În ce măsură o asemenea discuție este de actualitate, prioritară sau utilă – rămâne ca timpul și timpurile să vorbească!

Putem însă discuta despre condițiile necesare a fi îndeplinite într-un asemenea demers!

Pentru a scoate în evidență complexitatea unei asemenea acțiuni, folosesc experiența activității de peste zece ani în cadrul Întreprinderii de Automobile ARO Muscel Câmpulung! Poate ar trebui să ne amintim: ARO 24 – primul automobil de teren cu suspensie față independentă ; ARO 10 – primul automobil de teren cu suspensie integral independentă – realizări de excepție la nivel mondial ale inginerilor musceleni!

Producerea automobilelor de teren din familiile ARO 24, ARO 10 și ARO 32 (inclusiv variantele militare) a presupus constituirea unui sistem complex de cooperare economică ce cuprindea întreprinderi, institute de cercetare și chiar universități de profil. Pentru ultimele două categorii aș aminti doar Institutul Național de Motoare Termice, CCSITA Pitești și Universitatea Transilvania din Brașov!

Însă, pentru a schița o imagine sumară a cooperării „pe orizontală" în producția de automobile ARO (exportate în China, Columbia, Peru, Anglia, Franța, Spania, Belgia, Grecia, Polonia, Cuba, Ungaria, Algeria, Irak, Cehoslovacia, Vietnam, Portugalia etc., cu fabrică de automobile ARO 10 Ischia în Italia!) enumăr în continuare câteva localități din țară unde existau întreprinderi furnizoare de semifabricate și componente pentru automobilele ARO: Satu Mare - pompe de vacuum; Oradea – balamale, mânere și încuietori de uși, oglinzi; Arad – textile pentru tapițerie auto; ELBA Timișoara – faruri, lămpi de semnalizare; SINTEROM - Cluj-Napoca – bujii incandescente, bujii; Târgu Mureș – cablaje electrice; Mediaș – parbrize; Sfântu Gheorghe – reductoare; Sibiu – amortizoare; Săcele – aparatură de bord; Radiatoare Brașov – radiatoare; Tractorul Brașov – motoare D127, turnate din fontă (bloc motor, chiulase, cartere); Slatina – turnate din aluminiu; Scornicești – pompe de apă; Curtea de Argeș – motoare electrice, ștergătoare de parbriz; Câmpina – blocuri turnate pentru matrițe; Florești, Danubiana București – anvelope, camere de aer; Drăgășani – jante auto; Colibași – motoare; Topoloveni – cilindri de frână; Rucăr – eșapamente; Buzău – parbrize, geamuri; Râmnicu Sărat – discuri ambreiaj, garnituri de frână; Bârlad, Brașov, Alexandria – rulmenți; Vaslui – termostate; Roman – laminate, conducte de evacuare; Galați – laminate (table, bare); Piatra Neamț – semifabricate turnate din aluminiu; Policolor București, Victoria Făgăraș – lacuri și vopsele, diluanți, grunduri; Acumulatorul București – acumulatori; CATC Pitești, Fartec Brașov – garnituri de etanșare; Bacău, Brașov – elemente de asamblare (șaibe, șuruburi, piulițe etc.) și numeroase altele!

Proiectarea, omologarea, fabricarea acestor componente ale automobilului ARO - ce echipau și variantele militare ale acestuia – demonstrează atât competența inginerilor români, dar mai ales dezvoltarea unei rețele naționale de întreprinderi implicate în realizarea acestui produs complex! Aceste sisteme de cooperare economică au fost realizate pornindu-se aproape de la zero, în timp, cu responsabilitate și multa muncă, simț al datoriei, dar, mai ales cu o pregătire profesională inginerească de înalt nivel!

Așadar, se poate! Este posibilă o nouă dezvoltare importantă a industriei naționale de autovehicule de diverse tipuri! Dar, îndeplinirea unei condiții prealabile este indispensabilă: asigurarea unui nivel ridicat de pregătire profesională tinerilor inginerii! Iar în această direcție, rolul universităților ce formează ingineri în domeniul „Ingineria autovehiculelor" este fundamental! Dar, efortul colectiv generează progres! Pentru binele tuturor!

Prof. univ. dr. ing. Minu MITREA
Secretar General SIAR
Academia Tehnică Militară „Ferdinand I"

SUMAR „INGINERIA AUTOMOBILULUI" NR. 67

REGISTRUL AUTO ROMÂN

Director general
Alina NIȚĂ
Director tehnic
Ing. Cristian Viorel BUCUR

Șef Compartiment Comunicare și Redacție Revistă Auto Test
Roxana DIMA

Redactori
Radu BUHĂNIȚĂ
Emilia PETRE
George DRUGESCU

Contact:
Calea Griviței 391 A,
sector 1, cod poștal 010719,
București, România
Tel/Fax: 021/202.70.00
E-mail: autotest@rarom.ro
www.rarom.ro
www.autotestmagazin.ro

SIAR

Contact
Facultatea de Transporturi
Universitatea Politehnica
București
Splaiul Independenței 313
Sala JC 005, Cod poștal 060042, sector 6, București, România
Tel/Fax: +40.753.081.851
E-mail: siar@siar.ro
www.ingineria-automobilului.ro
www.siar.ro
https://www.facebook.com/SIAR.FISITA/

TIPAR
S.C. TIPOGRAFIA PROD COM S.R.L.
Str. Lt. Col. Dumitru Petrescu 20, Tg. Jiu
Jud. Gorj

The articles published in „Ingineria automobilului" magazine are indexed by Web of Science in the „Emerging Source Citation Index (ESCI)" Section.
(Journal Citation Indicator: JCI rIA = 0.02/2021)

Articolele publicate în „Ingineria automobilului" sunt incluse în ***Romanian Journal of Automotive Engineering*** *(ISSN 2457 – 5275) – revista SIAR în limba engleză.*
Revistele SIAR sunt publicate la adresa ***www.ro-jae.ro***

ON THE NUANCING OF COMPRESSION AND EXPANSION RATIOS

DESPRE NUANȚAREA NOȚIUNILOR DE RAPORT DE COMPRIMARE ŞI RAPORT DE DESTINDERE

REZUMAT: *În prezent, în ciuda dezavantajelor sale, motorul cu ardere internă este încă cea mai convenabilă alegere pentru mobilitatea rutieră. Dintre cele două tipuri de motoare cu ardere internă ce pot fi folosite pentru autopropulsie, cel cu aprindere prin scânteie este cunoscut ca fiind mai puțin eficient din punct de vedere termodinamic. Prin urmare, unele tehnologii sunt considerate în prezent relevante pentru a genera ameliorarea energetică a acestuia, cum ar fi: raportul de comprimare variabil, distribuția variabilă și destinderea prelungită (ciclul Atkinson-Miller), eventual, cuplate cu turbo-supraalimentare.*
Pentru a înțelege pe deplin aceste tehnici, în primul rând, noțiunea de „raport de comprimare" ar trebui definită clar. În ceea ce privește definirea sa, în literatura de specialitate există un anumit grad de neuniformitate. Prin urmare, acest articol subliniază necesitatea standardizării pentru a evita orice confuzie care ar putea fi creată printr-o utilizare nepotrivită a acestui termen. Mai mult decât atât, având în vedere răspândirea recentă a utilizării ciclurilor cu destindere prelungită (Miller-Atkinson) la motorul cu aprindere prin scânteie, atunci, la fel de importantă este legătura dintre raportul de comprimare și cel de destindere. Astfel, următorii termeni sunt definiți clar în acest articol: raportarele de comprimare și destindere, rapoartele volumetrice ori geometrice de comprimare și destindere, rapoartele volumetrice ori geometrice efective de comprimare și destindere și raportul real de comprimare. Rezultate experimentale adecvate sunt de asemenea prezentate pentru a susține aceste definiții.
Keywords: *internal combustion engine, compression ratio, expansion ratio*


Prof. univ. dr. ing.
Adrian-Constantin CLENCI
adrian.clenci@upit.ro


Conf. univ. dr. ing.
Rodica NICULESCU

Universitatea din Pitești, Departamentul Autovehicule și Transporturi, Str. Târgul din Vale, Nr. 1, 110040 PITEŞTI, România

1. OVERVIEW

In spite of the development of electrical vehicles, the internal combustion (IC) engine still remains today an appropriate and attractive solution for ensuring road mobility. Engines have improved dramatically over the past two decades, but current scientific developments suggest that there could be a reduction of 6% to 15% fuel consumption in the coming decade [1].

While the compression ignition (CI) engine has made enormous progress in recent years concerning fuel economy, the spark ignition (SI) engine still lags behind from this point of view. Nevertheless, this gap can be reduced using different technical solutions: variable compression ratio (VCR), downsizing via turbocharging, variable valve actuation (VVA), Atkinson-Miller over-expanded cycles, some of them already applied in mass production. However, the authors believes that in order to fully understand these techniques, first of all, the notion of *"compression ratio (CR)"* should be clearly defined [2]. Surely, for some readers, the previous statement could be surprising but as it will be seen below, there are many nuances which sometimes make difficult the complete understanding of any of the techniques specified before.

For instance, it is known that during most of its life, a passenger car engine is run under low loads and speeds. At these operating points, the overall IC engine efficiency decreases from the peak values (about 35-40%) to dramatically lower values (sometimes even below 10%). Low loads on SI engine are traditionally accomplished by means of a throttle plate which creates additional pumping losses. Thus, one may state that, in its turn, this decreases the *compression peak pressure*, hence the *"effective compression ratio (ECR)"*. The latter notion is quite often encountered in scientific literature [3–10] but equally often, one may find different understandings of this notion.

As a further example, figure 1a, [5][10], shows the ECR contours of a typical SI engine, according to engine speed and brake mean effective pressure (BMEP) but without mentioning how ECR was estimated.

The same happened in paper [9], which shows the effect of increasing the *"geometric compression ratio" (GCR)* from 8.5 to 12.5 upon the ECR, for which this author simply use the *compression ratio (CR)* name (figure 1b,c).

Regarding the CR definition, considering this notion is at the basis of the whole thermodynamic improvement of the IC engine, the authors believes that a *nuanced understanding* would be just needed. Moreover, considering the recent spreading of the use of over-expanded cycles (Miller-Atkinson) in SI engine, then, equally important is CR's connection with *expansion ratio (ER)*. On this particular subject, Heywood in his book [11] felt the need to introduce the notions of "actual *volumetric compression* and *expansion ratios*", which, it is said "are both less than the *nominal compression ratio*" used the term "*geometric effective compression ratio" (GECR)* in order to be able to characterize the *actual compression process* in real engines, which does not effectively start until the intake valves close.

Thus, further to the analysis of literature, a clear conclusion can be drawn, i.e., a certain degree of non-uniformity exists in using these simple notions of compression and expansion ratios [3–11]: *geometric, volumetric, actual, nominal, effective compression or expansion ratios...* Certainly, some of them are synonymous, however, the authors feel there is a need for standardization in order to avoid any confusion that might be created by a misleading use of this term. The work presented below is the result of many reflexions of the authors, some of them being included in different papers published by now [2][14][15][16].

2. COMPRESSION AND EXPANSION RATIOS IN THE IDEAL THERMODYNAMIC CYCLES

Expansion stroke being the only one producing work, it's of course interesting to discuss about its *expansion ratio (ER)*. Obviously, the higher *the volumetric expansion ratio (VER = GER =* ε_e *)*, the higher the efficiency. Actually, very evocative for this matter is the ideal cycle of Lenoir, which does not have a compression stroke (figure 2).

Its thermodynamic efficiency was then defined as a function of *volumetric or geometric expansion ratio (VER =* ε_e*)*, as shown below:

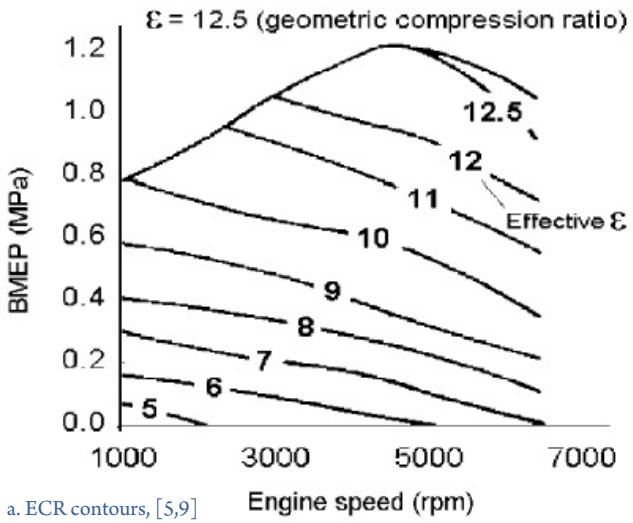

a. ECR contours, [5,9]

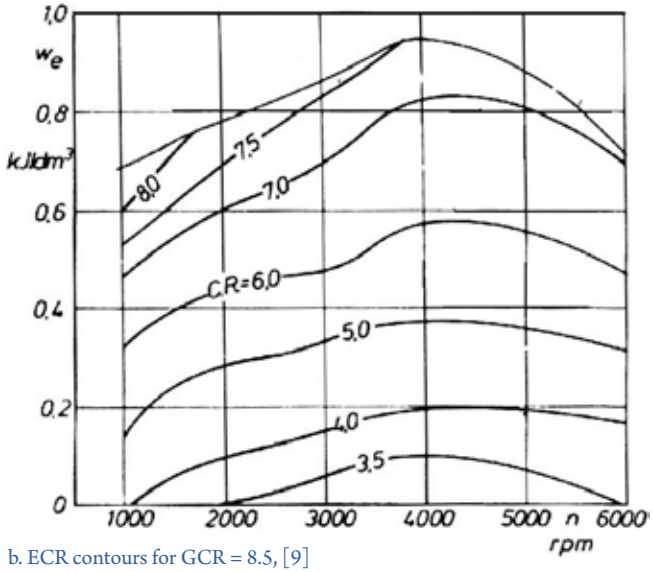

b. ECR contours for GCR = 8.5, [9]

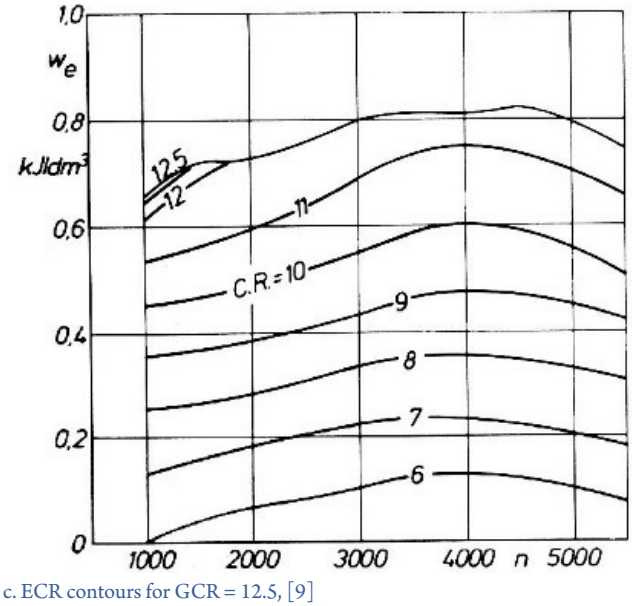

c. ECR contours for GCR = 12.5, [9]

Fig. 1. "Effective compression ratio" according to load and speed conditions

$$\eta_{th}=\frac{W}{Q_C}=\frac{\oint pdV}{Q_C}=\frac{A_{cycle}}{Q_C}=\frac{Q_C-|Q_{CS}|}{Q_C}=1-\frac{|Q_{CS}|}{Q_C}=1-\frac{c_p(T_4-T_2)}{c_v(T_3-T_2)}=$$

$$=1-\gamma\cdot\frac{(T_4-T_2)}{(T_3-T_2)}=1-\gamma\cdot\frac{T_2\left(\frac{T_4}{T_2}-1\right)}{T_2\left(\frac{T_3}{T_2}-1\right)}=1-\gamma\cdot\frac{\varepsilon_e-1}{\varepsilon_e^{\gamma}-1}, \quad (1)$$

where:

W[J] – mechanical work,

Q_C[J], Q_{CS}[J] – heat released from combustion and heat given to the cold source

A_{cycle} [J] – thermodynamic diagram area

c_p[J/kg/K], c_v[J/kg/K] – specific heat at constant pressure and volume

T[K] – temperature

γ[-] – ratio of specific heats

ε_e – volumetric expansion ratio

Then, if taking into consideration the Otto or Beau de Rochas ideal thermodynamic cycle (figure 3), one may notice the fact that *the volumetric expansion ratio (VER = ε_e)* is equal with *the volumetric or geometric compression ratio*[1] *(GCR = ε_c)*: piston goes up, air is compressed, piston goes down (same distance), air expands.

$$\varepsilon_c=\frac{V_{max}}{V_{min}}=\frac{V_1}{V_2}=\frac{V_4}{V_3}=\varepsilon_e, \quad (2)$$

where:

V_1, V_2, V_3, V_4 [m^3] – the volumes at the beginning and the end of compression and, respectively, expansion strokes

This makes possible the writing of its thermodynamic efficiency as follows:

$$\eta_{th}=1-\frac{1}{\varepsilon_e^{\gamma-1}}=1-\frac{1}{\varepsilon_e^{\gamma-1}} \quad (3)$$

As it is well known, the worldwide spread expression of Otto's thermodynamic efficiency is expressed as a function of ε_c and not as a function of ε_e. This might not be of any interest in Otto's engines but the moment when the over-expanded cycles (Miller-Atkinson cycles) are taken into consideration, it is needed to include them both. Actually, the two (ε_c and ε_e) should always be taken as a pair even though in some cases (such as Otto cycle) they are equal [14][15][16].

Coming back to the *compression ratio (CR)*, normally, it should be defined more as a ratio between pressures at the end and the beginning of the compression stroke (p_2, p_1) than as ratio of the corresponding volumes:

$$\tau_c=\frac{p_2}{p_1} \quad (4)$$

Perhaps a confusion was created because the *volumetric or geometric compression ratio (GCR)* is very often baptized as simply the *compression ratio (CR)*, which is defined by relation (2). The assimilation between the *pressure ratio* and *GCR* may be explained by using the ideal cycle featuring an isentropic compression of an ideal gas where there is a connection between the two of them as shown below:

1. *In this article, the authors preferred to use the acronym GCR for the volumetric or geometric compression ratio rather than VCR, in order to avoid a possible confusion with the general acceptance of VCR acronym, which stands for "variable compression ratio". However, for the geometric or volumetric expansion ratio, since there is no other widely used acronym to overlap with, the author uses the acronym VER.*

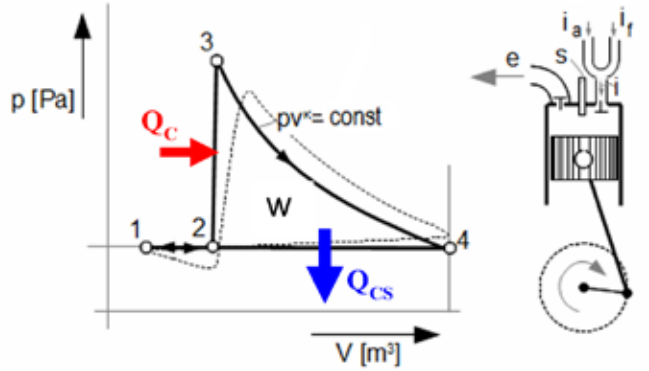

Fig. 2. Lenoir ideal thermodynamic cycle

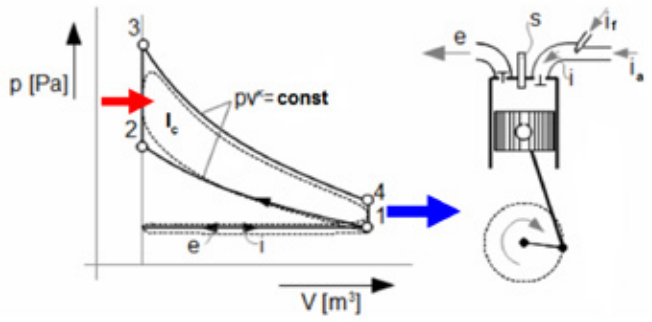

Fig. 3. Otto/Beau de Rochas ideal thermodynamic cycle

$$\tau_c = \frac{p_2}{p_1} = (\varepsilon_c)^{\gamma} \quad (5)$$

This connection exists also in case of the real compression if, instead of using γ, the polytropic coefficient (k) is used:

$$\tau_c = \frac{p_2}{p_1} = (\varepsilon_c)^{k} \quad (6)$$

where:

$$k = \frac{\ln(\tau_c)}{\ln(\varepsilon_c)} \quad (7)$$

In fact, for the well-being of the energetic performance of any SIE, what is important to know is rather how many times the pressure at the end of compression stroke increased in respect to the one from its beginning, and not the corresponding volumes ratio, which is known as *geometric or volumetric compression ratio, GCR*. Nevertheless, since this one is a *simple geometric parameter*, which can be easily measured and known, it is preferred to use the volumes ratio rather than the pressures ratio which is variable with engine load and speed. Moreover, another reason of using the volumes ratio is that the thermodynamic efficiencies of the ideal cycles are directly connected to them, as shown in figure 4.

The connection presented in figure 4 explains the continuous strive of engine manufacturers to increase the *geometric or volumetric compression ratio (GCR)*. Figure 5 pictures the evolution of *GCR* in time starting with the very first application of the german Nicolaus Otto and the french Beau de Rochas and showing some figures of exception (e.g. the interesting May-Fireball combustion chamber from 1978, which allowed a *GCR* of 14.3 or the Mitsubishi's worldwide premiere of stratified gasoline direct injection system allowing a *GCR* of 12.5 or more recently, the Mazda's "Sky Active" technology able to operate a SIE at a *GCR* of 14) [2][16].

Proceeding further with the discussion on the improvement of the thermodynamic efficiency of the ideal cycles, let's focus again on Otto or Beau de Rochas cycle (figure 3): *the in-cylinder expansion is not complete since the pressure at its end is still higher than the atmospheric pressure* ($p_4 > p_1 = p_{atm}$). This observation serves for supporting the conclusion formulated with the relation 3: the higher the *volumetric expansion ratio* the higher the thermodynamic efficiency.

Consequently, since the knock and NO_x are affected by the gas temperature and pressure at the end of the compression stroke, in other words by the *geometric or volumetric compression ratio (GCR)*, while the thermodynamic efficiency of the cycle is determined by the work during the expansion stroke, a better way to increase the efficiency is to have higher

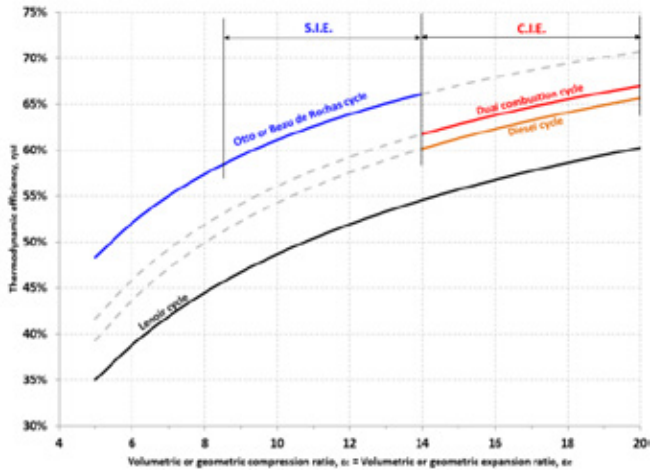

Fig. 4. Thermodynamic efficiency vs. volumetric ratios

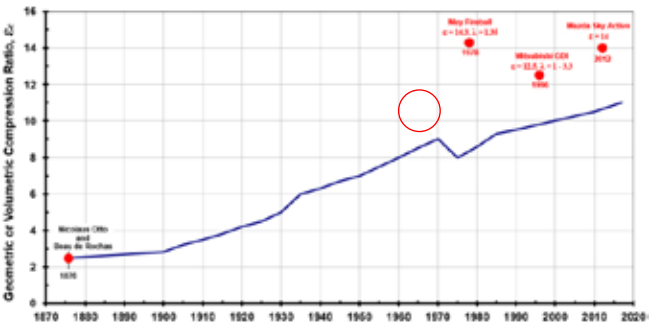

Fig. 5. Geometric compression ratio evolution in time[2]

expansion ratios rather than higher compression ratios [14]. This is the reasoning behind the concept of more-, over- or higher expansion cycle. The original idea belongs to the British engineer J. Atkinson (1886), who built an interesting engine capable of longer expansion and exhaust strokes, relatively to intake and compression strokes (figure 6).

From a theoretical point of view, the above-mentioned observation on the expansion stroke's (in)completeness invites to an extension of the expansion to atmospheric pressure, which leads to the definition of the maximum volumetric expansion ratio, ε_{emax}, [15][16].

2. *The "short" downward evolution in figure 5 (see the red circle) marks the moment of TWC introduction (in USA, especially), which required a lead-free gasoline; therefore, the GCR had to decrease in order to avoid the knocking occurrence; shortly after that event, the gasoline started to incorporate other anti-knocking lead-free additives, therefore, the GCR continued to increase.*

With $\lambda = \frac{p_3}{p_2}$, one may find ε_{emax} for a given geometric or volumetric compression ratio, ε_c:

$$\varepsilon_{emax}^{\gamma} = \frac{p_3}{p_5} = \frac{\lambda \cdot p_2}{p_5} = \frac{\lambda \cdot p_1 \cdot \varepsilon_c^{\gamma}}{p_5} = \lambda \cdot \varepsilon_c^{\gamma} \Rightarrow \varepsilon_{emax} = \varepsilon_c \cdot \lambda^{\frac{1}{\gamma}} \quad (8)$$

Therefore, *the rate of over-expansion* may be defined as follows [15][16]:

$$\tau_{oe}[\%] = 100 \cdot \frac{\varepsilon_e - \varepsilon_c}{\varepsilon_{emax} - \varepsilon_c} \quad (9)$$

The thermodynamic efficiency of the Atkinson cycle is given by the following relation:

$$\eta_{th} = 1 - \frac{1}{\varepsilon_c^{\gamma-1}} \cdot \frac{(\gamma-1)\cdot\left(\frac{\varepsilon_c}{\varepsilon_e}\right) + \lambda \cdot \left(\frac{\varepsilon_c}{\varepsilon_e}\right)^{\gamma-1} - \gamma}{(\lambda-1)} \quad (10)$$

Table 1 presents the improvement of the thermodynamic efficiency when employing the over-expansion technique (the calculations were done for different ε_c and for λ=3 and γ=1.4.

A simpler solution to implement the over-expansion in the classical piston combustion engines was proposed by Miller in 1947. Miller cycle differs from Otto or Beau de Rochas cycle by delaying the inlet valve(s) closing (IVC) well into the compression stroke; thus, till the IVC moment, the air is able to flow back into the inlet manifold (1'-1 phase in figure 7). The *effective compression* (1-2 phase in figure 7) will be activated during the remaining compression stroke, when the intake valve(s) will be closed. The result is the artificial decrease of the *geometric or volumetric compression ratio* relatively to *geometric or volumetric expansion ratio*, which remains the same. In this way, the compression and expansion are differentiated (see the evolutions 1-2 and 3-5 in figure 7).

Consequently, since the substantial start of compression process varies with the IVC timing, as mentioned in section 1, in order to avoid any confusion, some terms need to be redefined or nuanced [2]:

1. ε_{ec}, *volumetric or geometric effective compression ratio (GECR)*[3], which is defined as the ratio between the volume above the piston when IVC occurs and the volume above the piston when it is at top dead center (TDC):

$$GECR = \varepsilon_{ec} = \frac{V_{IVC}}{V_{TDC}} \quad (11)$$

2. since for Miller or Atkinson applications, the Otto or Beau de Rochas term *"geometric or volumetric compression ratio"* defined as the ratio between the volumes at BDC and at TDC is not relevant anymore for the compression stroke, perhaps it's better to call it simply *"volumetric ratio (VR)"*, ε; certainly, this is only relevant to characterize the expansion stroke; therefore, $\varepsilon=\varepsilon_e$.

Obviously, the *GECR* is lower than the *volumetric ratio (VR)*, which is equal to the *volumetric expansion ratio (VER)*:

$$GECR = \varepsilon_{ec} < \varepsilon = VR = \varepsilon_e = VER \quad (12)$$

The Miller cycle can also be implemented by closing the intake valve(s) before TDC position, resulting into the so-called Early IVC (see figure 8).

Actually, after this early intake valve closure (EIVC), an "expansion" of the fresh air is performed (see the evolution 1'-1" in figure 8) with a bit of effort from the engine's side, which theoretically is recovered in the first part of the compression stroke (see the evolution 1" – 1' in figure 8) when the pressure rises from the sub-atmospheric level to the atmospheric value occuring in the IVC moment. Thus, here, as well, the GECR is given by the IVC moment.

Table 1. Efficiency improvement through over-expansion

Volumetric compression ratio εc	Volumetric expansion ratio εe	Rate of over-expansion τoe [%]	Thermodynamic efficiency ηth [%]	The percentage improvement Δηth [%]
8	8	0	56.5	0
	13	52	62.6	10.8
	17.5	100	63.7	12.8
10	10	0	60.2	0
	16	51	65.7	9.1
	21.9	100	66.8	11.0
12	12	0	63.0	0
	19	49	68.0	7.9
	26.3	100	69.1	9.73

3. COMPRESSION RATIO IN THE REAL ENGINE CYCLES

When performing the cyclic analysis in the previous section, during the intake and exhaust processes no energy spent or required was considered, i.e., they are carried out without loss of energy, therefore, compression always starts at atmospheric pressure. In reality, these processes are characterized by an energy loss, usually known as *pumping loss*, which increases as the engine load decreases (in figure 9, it is illustrated by the negative low red loop). As pointed out in section 1, this is the result of power output control by means of throttling the fresh mixture flow, whose most important side effect in authors' opinion is the decrease of the *real compression ratio (RCR)* when reducing the load.

The Miller technique allows the throttle-free load control if using a VVA technique able to continuously adapt the IVC as presented in figure 10, [17].

Both cases presented in figure 10 are characterized, amongst others, by a continuously *variable geometric effective compression ratio (GECR)*. The advantage is indeed an important reduction of the pumping losses; however, this load control method remains a quantitative one, therefore, it still causes a reduction of the *real compression ratio (RCR)* with engine load. If taking for this notion the definition given by relation (4) then, considering that the pressure at the end of the compression stroke (p_2) is the effect of everything occurring before and during the compression process, it results that the decrease of the *real compression ratio* with engine load means the reduction of this p_2 pressure. The explanation for this reduction is simple: on the one hand, in the real compression processes, the starting point of compression stroke lowers with load (i.e., the lower the engine load, the lower the pressure at the beginning of compression; however, the decreasing of p_2 with engine load is faster than the one of p_1) and, on the other hand, the reducing mixture mass when load decreases accomplished by quantitative load control methods (e.g., throttling when load decreases) will occupy the same volume at the end of compression stroke (the lower the engine load, the lower the mass in the cylinder during the compression). A counteracting technique for this fundamental drawback of the SI engine is to have the possibility to vary the *geometric compression ratio (GCR)*: it increases as the load level decreases, i.e., the minimum value of *GCR* is imposed at full load in order

3. *Out of the multiple designations, the authors prefer "geometric effective compression ratio": **"geometric"** as it is still a ratio between volumes; **"effective"** as it is about the **effective** compression process, which starts with IVC moment; moreover, the term **"effective"** is frequently used in designating engine's parameters such as (indicated or brake mean **effective** pressure, **effective** power etc); thus, **"effective"** reflects the actual or the real value (the one which is): in our case, the real volumetric or geometric value of compression ratio.*

4. *The "short" downward evolution in figure 5 (see the red circle) marks the moment of TWC introduction (in USA, especially), which required a lead-free gasoline; therefore, the GCR had to decrease in order to avoid the knocking occurrence; shortly after that event, the gasoline started to incorporate other anti-knocking lead-free additives, therefore, the GCR continued to increase.*

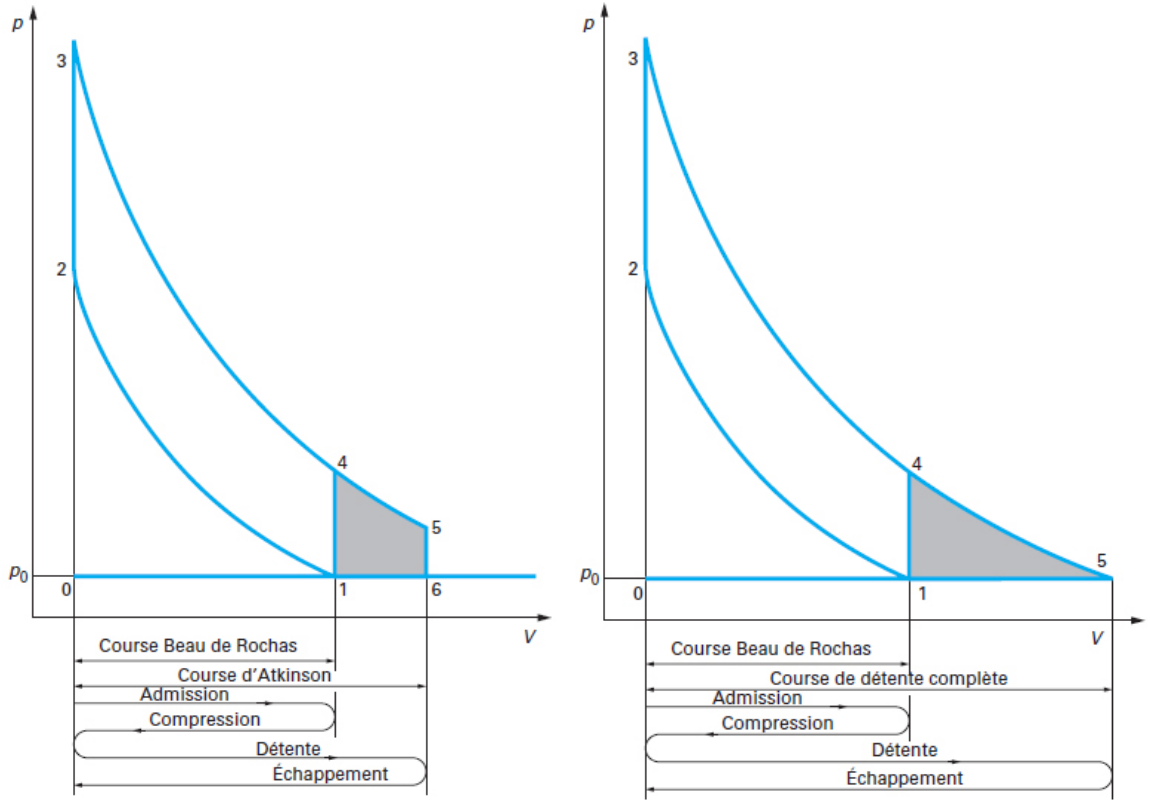

a. (still) incomplete expansion ($p_5 > p_0$) b. complete expansion ($p_5 = p_0$)

Fig. 6. Atkinson cycle, [15,16]

to avoid knocking, while its maximum value is chosen for fuel economy reason at idle operation. There are many ways to achieve this goal, most of them being presented in [16].

Coming back to the *real compression ratio (RCR)*, in the authors' view, it refers to the *intensity of compression*. However, the latter is influenced by many factors, amongst which load level, speed of rotation, intake valve law etc. The term, which could give a real image to the *intensity of compression* is, as already stated above, the pressure at the end of compression (p_2). Obviously, its value is an effect of all phenomena occurring between the beginning and the end of compression (wherever or whenever these might happen). Therefore, relation (4) is what's needed for defining the *real compression ratio*. Nonetheless, from practical standpoint, it is rather more interesting to express it in unities of *geometric compression ratio (GCR)* as shown in figure 1. To do so, the authors propose to *"reduce"*[5] the *real compression process* to an isentropic compression process, specific to the ideal Otto or Beau de Rochas cycle, characterized by the same value at its end as in the real situation (figure 11), [2]. Thus, in the situation of the ideal cycle to which the *"reduction"* operation was performed, the compression process starts from atmospheric pressure, p_0 and at the end, arrives to the p_2 pressure, measured on the real cycle. Consequently, the *real compression ratio expressed in unities of GCR* (τ_{rc})[6] corresponds to the *geometric compression ratio* of the ideal cycle to which the *"reduction"* operation was done:

$$p_1 \cdot V_1^{\gamma} = p_2 \cdot V_2^{\gamma} \overset{p_1=p_0}{\Longrightarrow} \left(\frac{p_2}{p_0}\right)^{\frac{1}{\gamma}} = \frac{V_1}{V_2} = \frac{Vmax_i}{V_{min}} = \tau_{rc} = RCR, \quad (13)$$

Certainly, the *real compression ratio (RCR)* found with relation (14) is getting smaller as the load level decreases; since the same combustion chamber volume is kept in both situations (V_{min} from figure 11), it results that the ideal cycle's maximum volume ($Vmax_i$) is in the same dependence with the load, as well. Equally, the following inequality holds true:

$$Vmax_i < Vmax_r, \quad (14)$$

where $Vmax_r$ is real cycle's maximum volume.

For a real combustion cycle, the authors proposal is to to determine the *real compression ratio (RCR)* relies on considering the end of compression as the ignition point; afterwards, the associated isentropic compression, containing this ignition point, should be found out, as it is shown below:

$$RCR = \tau_{rc} = \left(\frac{p_i}{p_0}\right)^{\frac{1}{\gamma}} \cdot \left(\frac{V_i}{V_2}\right), \quad (15)$$

where p_i, V_i are the pressure, respectively the cylinder volume measured at the ignition point.

Another way of having an image[7] of the *real compression ratio (RCR)* expressed in unities of *GCR* is to use the *filling coefficient/efficiency* (η_v). Indeed, since the pressure at the end of compression stroke is influenced

5. *NB. The „reduction" operation is a common practice in mechanical engineering (e.g., the obtaining of an automobile's equivalent dynamic model, „reduced" to the crankshaft's rotational motion; in this case, the automobile's translational mass is replaced with a fictional rotational mass, equivalent from energetic standpoint)*

6. *The author preferred to use τ for the real compression ratio instead of ε as it is related with pressures, as initially introduced by relation (4); then, the subscript "rc" was used to underline it's about the "real compression" ratio. Thus, in this work, ε designates a volumetric or geometric ratio, which in one way or another characterizes the compression and expansion processes, while τ is used to designate rather a pressure ratio.*

7. *Obviously, even though we are talking about the* ***real compression ratio (RCR)****, the values obtained by using the proposed methods are simply an "****image****". In fact, because of the spark ignition engine's specificity, the authors simply wanted to have a method to determine the* ***RCR*** *on the whole engine's operating area; hence, relations (16) and (17).*

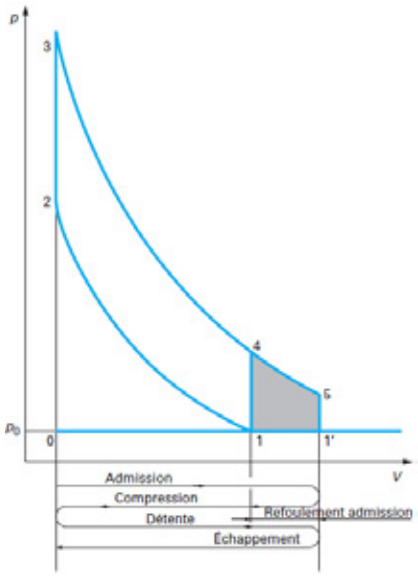

Fig. 7. Late IVC Miller cycle

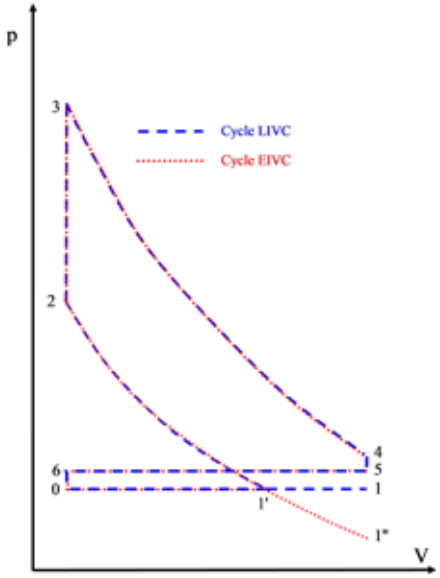

Fig. 8. Late vs. Early IVC Miller cycle

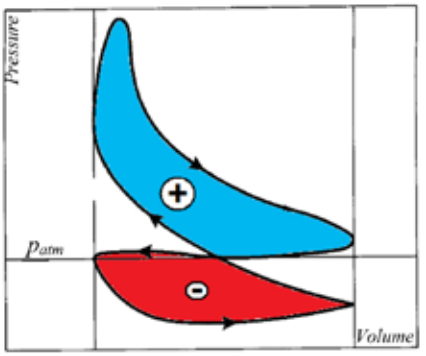

Fig. 9. Real engine cycle

Table 2. Engine data

Number of cylinders	4 in line
Bore [mm] x Stroke [mm]	78 x 83.6
Connecting rod length [mm]	145
Geometric compression ratio	10.7
Combustion chamber volume [cm3]	41.2 cm3
Max. power [kW] @ speed [rpm]	84@5800
Max. torque [Nm] @ speed [rpm]	156@4000

by the mass trapped inside the cylinder, then, why not having an image of the *RCR* by simply multiplying the *GCR* with the *filling coefficient*, as given below:

$$RCR = \tau_{rc} = \varepsilon_c \cdot \eta_v \quad (16)$$

4. CASE STUDY: FINDING THE REAL COMPRESSION RATIO FOR A GIVEN ENGINE

To find the *RCR* map (i.e., the values of RCR for the whole engine's operating area), a naturally aspirated SI engine whose technical definition is given in table 2 was used.

The tests were performed on a usual engine test bed and consisted in performing a sweep over the whole operating area with a 500 rpm speed step between 1500 and 6000 rpm and a load step of 1 bar of brake mean effective pressure (BMEP) between minimum and maximum value for each considered speed. Hence, 116 operating points resulted (figure 12). Average time for each operating point was about 6 minutes: 1 minute for reaching the operating point, 3 minutes waiting time for reaching a stable operating point and the rest was the time needed to acquire 2000 engine cycles. Consequently, almost 12 hours were spent at the engine test bench for gathering all the experimental data. Finally, for each operating point, the following was taken:

- a relevant indicated diagram through averaging 2000 engine cycles,
- the ignition advance, in order to obtain the pressure, respectively, the cylinder volume at the ignition point,
- the filling efficiency.

Consequently, tables 3 and 4 present the pressure and the cylinder volume at the ignition point while table 5 shows the RCR values obtained by applying relation (15).

Table 6 shows the filling efficiency of the investigated engine over the whole operating range serving for the calculation of RCR with relation (16).

A graphical illustration of the RCR maps calculated with relations (15) and (16) is given in figure 13.

By comparing the two images from figure 13, one may see that the proposed relation (15) gives results which are comparable to the ones obtained by using the filling efficiency. This supports the above statements from section 3, according to which, the *RCR* calculation based on pressure at the end of compression encapsulates all the phenomena occurring before and during the compression process.

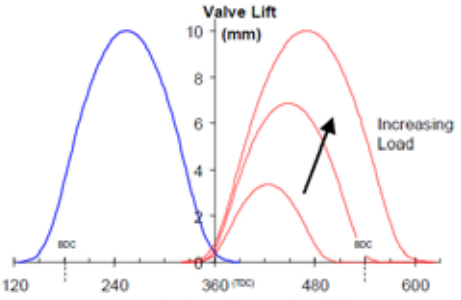

a. EIVC strategy

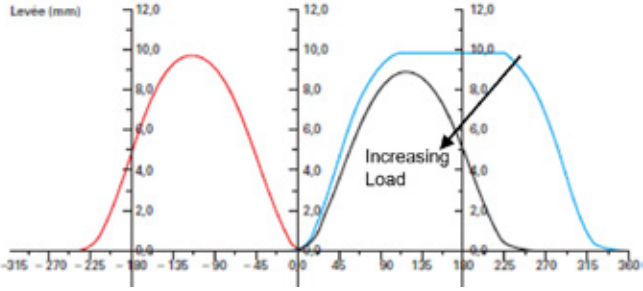

b. LIVC strategy

Fig. 10. Throttle-free load control methods via VVA

5. SUMMARY AND CONCLUSIONS

This article is the result of authors' reflexions, which started during the period 1997-2003 when the SI engine's industry witnessed an explosion of VCR solutions, some of them ready for the mass production at that time. Then, they continued and grew in time till the form presented subsequently. In fact, in this article, the authors tried to standardize somehow some basic notions from engine's thermodynamics (compression and expansion ratios) whose good understanding influences the good understanding of techniques such as VCR, VVA, Atkinson-Miller cycle. Surely, the notions are not complex; however, there are many nuances and moreover, in the existing literature, a certain degree of non-uniformity exists, hence the author's preoccupation.

Thus, the main findings of this study are summarized as follows:

• *expansion ratio* (ε_e), which is not often met in the (Romanian) books of engines thermodynamics was explicitly introduced and defined;

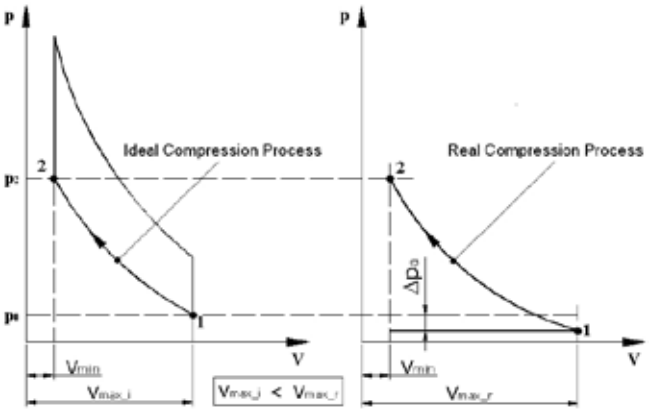

Fig. 11. „Reducing" the real compression process to an ideal (isentropic) one

Table 3. In-cylinder pressures [bar] at the ignition points

		SPEED [rpm]										
		1250	1500	2000	2500	3000	3500	4000	4500	5000	5500	6000
BMEP [bar]	1	2.300	2.009	1.674	1.641	1.574	1.692	1.944	2.252	2.572	2.686	2.455
	2	3.768	3.266	2.745	2.753	2.640	2.735	2.974	3.285	3.638	3.724	3.496
	3	5.430	4.564	3.989	4.260	4.236	4.080	4.203	4.295	4.910	4.991	4.650
	4	7.210	5.692	5.403	5.619	5.867	5.452	5.351	5.644	6.195	6.390	5.686
	5	9.697	7.157	6.797	7.115	7.206	6.812	6.417	6.796	7.448	7.588	7.011
	6	12.666	10.206	8.133	8.269	8.400	7.971	8.117	7.674	9.040	8.995	8.822
	7	16.519	13.723	11.029	9.848	9.689	9.225	9.020	9.273	10.800	11.179	10.973
	8	19.418	15.999	13.432	11.644	11.464	10.973	10.341	10.667	12.400	12.538	13.001
	9	-	19.925	16.292	13.199	12.472	12.465	12.372	13.123	15.346	15.349	15.237
	10	-	20.981	19.488	16.570	14.529	14.118	15.084	15.488	16.984	17.971	-
	11	-	-	20.204	17.484	15.225	16.093	16.284	16.382	18.103	19.364	-
	12	-	-	-	-	-	-	17.372	-	-	-	-

Table 4. Cylinder volumes [cm3] at the ignition points

		SPEED [rpm]										
		1250	1500	2000	2500	3000	3500	4000	4500	5000	5500	6000
BMEP [bar]	1	78.86	88.49	103.66	103.04	105.82	106.18	101.47	93.84	88.31	88.86	93.86
	2	72.21	81.45	90.47	86.83	90.25	90.23	88.68	84.08	80.67	80.27	84.96
	3	66.60	75.97	82.25	75.71	76.67	79.33	80.35	77.58	75.00	74.34	80.26
	4	62.14	71.14	74.34	69.01	68.01	72.06	74.98	72.45	70.55	70.29	76.62
	5	53.02	64.69	68.83	64.60	64.38	68.66	71.45	70.31	68.48	67.33	71.95
	6	45.94	54.37	63.47	61.53	62.41	65.89	65.97	68.81	63.13	64.83	65.76
	7	42.53	46.50	54.88	57.88	60.75	63.94	65.73	65.44	60.37	60.41	61.87
	8	41.28	44.78	50.40	55.45	57.76	61.18	64.23	63.40	58.99	58.43	57.96
	9	-	42.47	46.83	54.39	56.87	58.73	58.94	58.90	54.47	54.13	55.14
	10	-	41.78	44.23	48.84	54.75	56.30	55.93	56.11	52.82	51.88	-
	11	-	-	44.17	48.45	54.34	54.16	54.85	55.48	52.91	51.56	-
	12	-	-	-	-	-	-	54.20	-	-	-	-

Table 5. Real compression ratio (RCR) map

BMEP[bar]	SPEED [rpm]										
	1250	1500	2000	2500	3000	3500	4000	4500	5000	5500	6000
1	3.5	3.5	3.6	3.6	3.5	3.7	3.9	4.1	4.2	4.3	4.3
2	4.5	4.6	4.5	4.3	4.4	4.5	4.7	4.7	4.9	5.0	5.0
3	5.4	5.4	5.3	5.1	5.2	5.2	5.4	5.3	5.6	5.6	5.8
4	6.1	5.9	6.0	5.7	5.8	5.8	6.0	6.0	6.2	6.4	6.4
5	6.4	6.3	6.5	6.3	6.3	6.5	6.5	6.6	6.9	6.9	7.0
6	6.8	6.9	6.8	6.7	6.9	7.0	7.1	7.1	7.3	7.5	7.5
7	7.5	7.2	7.3	7.1	7.4	7.5	7.6	7.7	7.9	8.1	8.2
8	8.2	7.8	7.7	7.7	7.9	8.1	8.2	8.2	8.5	8.5	8.7
9		8.6	8.2	8.2	8.3	8.5	8.5	8.9	9.2	9.1	9.2
10		8.8	8.8	8.7	8.9	8.9	9.3	9.5	9.6	9.8	
11			9.0	8.9	9.1	9.4	9.6	9.8	10.0	10.2	
12							10.0				

Table 6. Filling efficiency map

BMEP[bar]	SPEED [rpm]										
	1250	1500	2000	2500	3000	3500	4000	4500	5000	5500	6000
1	0.178	0.178	0.177	0.180	0.184	0.191	0.199	0.208	0.215	0.227	0.230
2	0.249	0.249	0.255	0.253	0.256	0.262	0.268	0.276	0.283	0.293	0.304
3	0.314	0.314	0.316	0.319	0.321	0.330	0.338	0.347	0.353	0.363	0.375
4	0.383	0.383	0.384	0.384	0.386	0.398	0.407	0.416	0.422	0.435	0.438
5	0.456	0.450	0.453	0.452	0.453	0.464	0.477	0.484	0.493	0.505	0.507
6	0.540	0.522	0.519	0.520	0.518	0.532	0.548	0.553	0.565	0.579	0.577
7	0.635	0.606	0.589	0.588	0.584	0.600	0.615	0.623	0.639	0.654	0.656
8	0.742	0.683	0.661	0.658	0.653	0.669	0.685	0.695	0.710	0.709	0.735
9	-	0.777	0.740	0.726	0.723	0.739	0.766	0.773	0.794	0.789	0.817
10	-	0.832	0.829	0.811	0.796	0.813	0.847	0.853	0.854	0.868	-
11	-	-	0.868	0.863	0.846	0.881	0.920	0.888	0.917	0.943	-
12	-	-	-	-	-	-	0.962	-	-	-	-

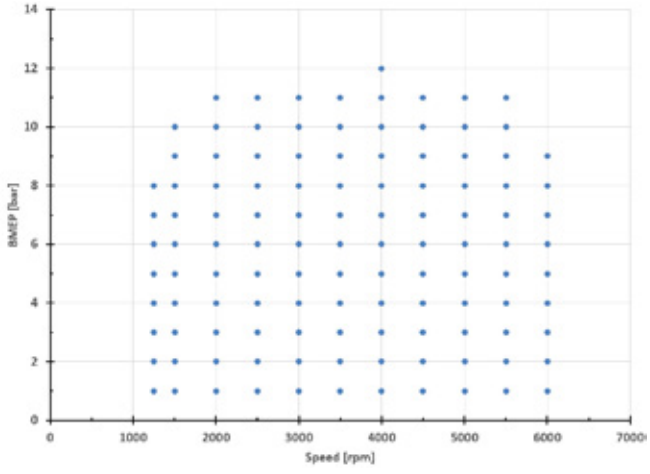

Fig. 12. Explored operating points

• a clear connection was made between *expansion ratio* and thermodynamic efficiency though most of the (Romanian) books of engines thermodynamics use only *compression ratio* notion;

• a differentiation between *volumetric expansion ratio* and *volumetric compression ratio* was given by introducing the Miller-Atkinson cycles, which to the author's knowledge is still not introduced as such in the Romanian books of thermodynamics;

• other expansion related parameters were also introduced: *maximum volumetric expansion ratio needed for a complete expansion* (ε_{emax}) and the *rate of over-expansion* (τ_{oe});

• a nuancing of the *compression ratio* was provided which per se is meant to provide solid premises for a good understanding of engine techniques such as VCR, VVA and Atkinson-Miller:

- *geometric or volumetric compression ratio* (ε_c)
- *geometric or volumetric effective compression ratio* (ε_{ec})
- *real compression ratio* (τ_{rc})

• an original method to quantify the *real compression ratio* was given

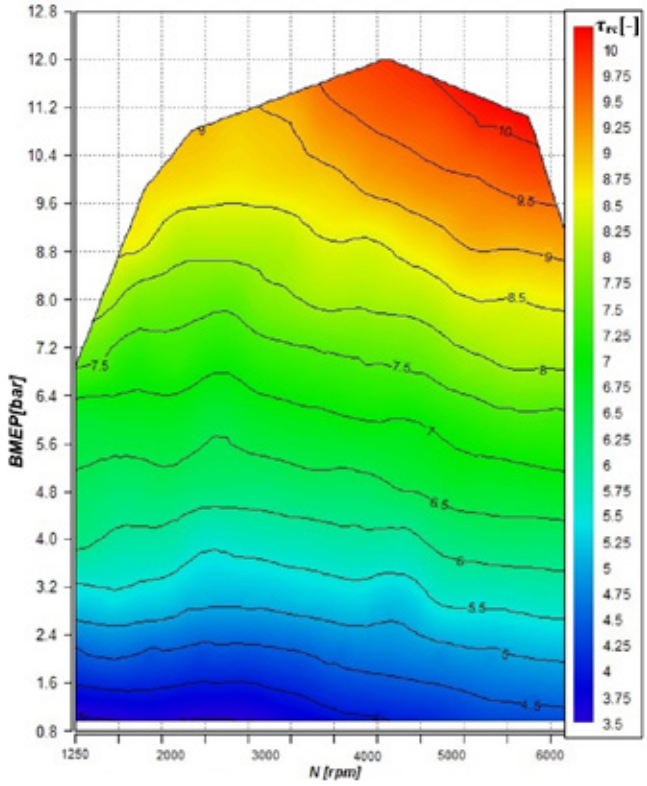

a. calculation with relation (15)

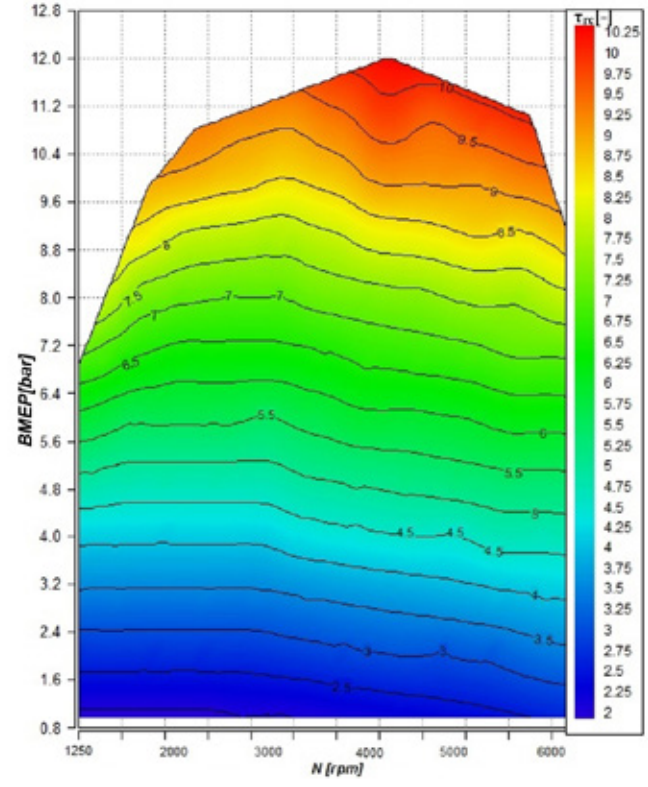

b. calculation with relation (16)

Figure 13. Real compression ratio (RCR) contours

together with a case study showing results based on experimental data; thus, the degradation of *real compression ratio* when the load decreases was clearly identified, supporting in a better way the works on the VCR topic. It is the authors' belief that whenever a certain degree of non-uniformity appears in our scientific endeavours, an approach such as the one presented here is required.

As for the future works on this topic, the authors plan to approach the case of a turbocharged spark ignition engine, in the attempt to characterize the whole compression and expansion processes (i.e., on the one hand, the whole compression formed by the process occurring first in the centrifugal compressor and then in the engine's cylinder and, on the other hand, the whole expansion taking place first in the engine's cylinder and then in the turbine).

Acknowledgements

The author is grateful to Professor Michel Feidt from University of Lorraine, France and dr. Pierre Podevin from Cnam Paris for the fruitful discussions on this topic. Equally, the authors thanks their Master student Mr. Irinel Stăncescu with whom the authors conducted the tests at the engine test bench, which served for his Master thesis, as well.

REFERENCES:

[1] A.M.K.P. Taylor, Science review of internal combustion engines, Energy Policy. 36 (2008) 4657–4667. doi:10.1016/j.enpol.2008.09.001.
[2] A. Clenci, R. Niculescu, On the compression ratio definition, in: SIAR (Ed.), 8th Int. Congr. ESFA, Organ. under FISITA Patronage, SIAR, Bucarest, 2009: pp. 49–55.
[3] J.H. Tuttle, Controlling Engine Load by Means of Late Intake-Valve Closing, SAE Tech. Pap. 800794. (1980). doi:10.4271/800794.
[4] J.M. Mallikarjuna, V. Ganesan, Optimization of inlet valve closure timing and clearance volume of a SI engine for better performance at part loads - A numerical and experimental approach, Indian J. Eng. Mater. Sci. 13 (2006) 307–321.
[5] O.A. Kutlar, H. Arslan, A.T. Calik, Methods to improve efficiency of four stroke, spark ignition engines at part load, Energy Convers. Manag. 46 (2005) 3202–3220. doi:10.1016/j.enconman.2005.03.008.
[6] B.R. de S. Ribeiro, Thermodynamic optimisation of spark ignition engines under part load conditions, Ph.D. Thesis. (2006).
[7] B. Ribeiro, J. Martins, Direct comparison of an engine working under Otto , Miller and Diesel cycles : Thermodynamic analysis and real engine performance, SAE Tech. Pap. (2007) 2007-01–0261. doi:10.4271/2007-01-0261.
[8] K. Stricker, L. Kocher, E. Koeberlein, D. Van Alstine, G.M. Shaver, Estimation of effective compression ratio for engines utilizing flexible intake valve actuation, Proc. Inst. Mech. Eng. Part D J. Automob. Eng. 226 (2012) 1001–1015. doi:10.1177/0954407012438024.
[9] D. Gruden, H. Richter, Torque characteristics and fuel efficiency of various gasoline engine concepts, SAE Tech. Pap. (1984). doi:10.4271/841284.
[10] F. Schäfer, R. van Basshuysen, Reduced Emissions and Fuel Consumption in Automobile Engines, Springer-Verlag Wien, 1995. doi:10.1007/978-3-7091-3806-9.
[11] J.B. Heywood, Internal Combustion Engine Fundamentals, 1988. doi:10987654.
[12] K. Stricker, L. Kocher, D. Van Alstine, G.M. Shaver, Input observer convergence and robustness: Application to compression ratio estimation, Control Eng. Pract. 21 (2013) 565–582. doi:10.1016/j.conengprac.2012.11.009.
[13] M. Klein, L. Eriksson, J. Åslund, Compression ratio estimation based on cylinder pressure data, Control Eng. Pract. 14 (2006) 197–211. doi:10.1016/j.conengprac.2005.03.022.
[14] A. Clenci, F. Ivan, R. Racota, Higher Expansion or Higher Compression at S.I.E.?, in: SIAR (Ed.), 7th Int. Conf. ESFA, Organ. under FISITA Patronage, SIAR, Bucharest, 2003.
[15] A. Clenci, P. Podevin, G. Descombes, Etude thermodynamique de la détente prolongée, in: SFT (Ed.), Colloq. Francoph. Sur l'Energie, Environnement, Econ. Thermodyn. COFRET'08, Nantes, 2008: pp. 11–13.
[16] P. Podevin, A. Clenci, Moteurs à taux de compression variable, in: Tech. l'Ingenieur, T.I., Techniques de l'Ingénieur, 2008: pp. 0–21.
[17] A. Biziiac, Cercetări privind ameliorarea performanțelor energetice ale unui motor cu aprindere prin scânteie prin realizarea variației înălțimii de ridicare a supapelor de admisie, Doctoral thesis, University of Pitesti, 2011.

ANALISYS OF A STEERING ROD IN THE PRESENCE OF PARAMETRIC UNCERTAINTIES

ANALIZA UNEI BIELETE DE DIRECȚIE ÎN PREZENȚA INCERTITUDINILOR PARAMETRICE

REZUMAT: *Această lucrare prezintă analiza unei bielete de direcție a unui autovehicul sub incertitudini parametrice, prin utilizarea atât a software-ului comercial FEA Abaqus, cât și a FEMCAS, un nou software dezvoltat pentru analiza structurală. Este descrisă abordarea teoretică, inclusiv modulul de analiză liniară cu incertitudini parametrice - simularea Monte Carlo, metoda perturbației și metoda Neumann. Metoda perturbației implică o extensie din seria Taylor a matricei de rigiditate și este o alternativă numeric mai puțin costisitoare la metoda Monte Carlo. Metoda Neumann aplicată în analiza elementelor finite este cunoscută în literatura de specialitate sub numele de Spectral Stochastic Finite Element Method și modelează incertitudinile folosind o metodă modificată de perturbație stochastică de prim ordin împreună cu o expansiune Karhunen-Loeve trunchiată în locul seriei Taylor. În absența incertitudinilor parametrice, s-a efectuat o analiză modală și o analiză a vibrațiilor forțate. Rezultatele de la FEMCAS au fost comparabile cu calculul teoretic, precum și cu Abaqus care arată o bună precizie a sover-ului. Sub incertitudini parametrice, s-a obținut o bună corelație între metodele Monte Carlo, Perturbație și Neumann. Cu toate acestea, metoda perturbației și metoda Neumann au obținut timpi de simulare mult mai mici, ceea ce a făcut ca aceste soluții să fie mult mai ieftine din punct de vedere computațional.*

Keywords: *FEA. frequency. dynamics. uncertainties. vibration. perturbation. Monte Carlo simulation*

S.l. dr. ing.
Gabriel-Cătălin MARINESCU[1]

Dr. ing.
Stefan CASTRAVETE[2]
scastravete@caelynx.ro

[1] Universitatea din Craiova, Departamentul de Autovehicule, Transporturi și Inginerie Industrială, Strada Alexandru Ioan Cuza, Nr. 13, 200585 CRAIOVA, România
[2] Caelynx Europe, Str. Păltiniș, Nr. 13E, 200128 CRAIOVA, România

1. INTRODUCTION

The parametric uncertainties are frequently considered in the analyses of various situations, like control of nonlinear processes, dynamics and mass balance, optimization of trajectories of robots or various physical predictions. For example, paper [1] approaches a procedure for the design of a robust controller for a nonlinear process, considering the various issues arising in the design. There are used the main theoretical results from the Literature about this topic. An extended model is set-up, linking performance and robustness to the control law, having as result a state feed-back control law which guarantees robust performance.

Paper [2] approaches a climate model tuning and presents an iterative automatic tuning method from the statistical science literature, referred as iterative refocusing that avoids many of the common pitfalls of automatic tuning procedures. It is based on optimization of a cost function, principally the over-tuning of a climate model due to using only partial observations. This avoidance comes by seeking to rule out pa-parameter choices that we are confident could not reproduce the observations, rather than seeking the model that is closest to them (a procedure that risks overtuning). Another example of the use of parametric uncertainties is presented in paper [3], where the behavior of continental-scale ice sheets is modeled and simulated. This is done under past, present, or future climate scenarios that are subject to several uncertainties from various sources. The sources include the conceptualization of the ISM and the degree of abstraction and parameterizations of processes such as ice dynamics and mass balance. The assumption of spatially or temporally constant parameters (such as degree-day factor, atmospheric lapse rate or geothermal heat flux) is one example. In paper [4], there is extended the notion of closed-loop state sensitivity by introducing the concept of input sensitivity and by showing how to exploit it in a trajectory optimization framework. It allows generating an optimal reference trajectory for a robot that minimizes the state and input sensitivities against uncertainties in the model parameters, thus producing inherently robust motion plans. The reference trajectories with Beziers curves are parameterized, and there are discussed the ways to consider linear and nonlinear constraints in the optimization process. A method for design of robust PI controllers is presented in paper [5]. It is based on plotting the stability boundary locus in (kp, ki) – plane and then parameters of stabilizing PI controllers are obtained. Paper [6] Approaches the traceability of imaging spectrometer data, the associated measurement uncertainties must be provided reliably. A new tool for a Monte-Carlo-type measurement uncertainty propagation for the uncertainties that originate from the spectrometer itself is described. For this, an instrument model of the imaging spectrometer ROSIS was used.

A generalized uncertainty principle is described in paper [7] that reviews some of the physical predictions of the GUP, and focuses on the bounds that present experimental tests can put on the value of the deformation parameter β. There are described a theoretical value computed for β, and comment on the vast parameter region.

This research studies the behavior of a cantilever beam in the presence of uncertainties using a novel software based on stochastic finite element method.

2. THEORETICAL CONSIDERATIONS

2.1 Finite element model

A steering rod of a vehicle is proposed [11].

The governing equations of motion are obtained using the Lagrange equation.

Steering rod (see Figure 1) is split into elements like in the Figure 2 (a) where one element is represented in Figure 2(b) [10].

Element displacements, $\tilde{u}(y,t)$, $\tilde{v}(y,t)$, and $\tilde{w}(y,t)$ are expressed in terms of nodal displacements u_i, v_i, w_i in directions x, y, z and nodal rotations β_i, α_i, γ_i around axes x, y, and z.

Equations for one element can be written in matrix form:

$$[M]^e\{\ddot{U}\}^e+[K]^e\{U\}^e=\{F\}^e \quad (1)$$

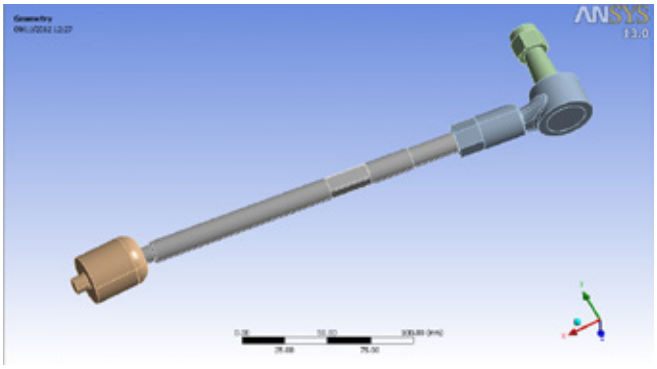

Fig. 1. Geometrical Model [11]

Assembling elements, we obtain:

$$[M]\{\ddot{U}\}+[K]\{U\}=\{F\} \quad (2)$$

where, [M] is mass matrix, [K] is stiffness matrix, {F} exterior applied force vector, {U} is displacement vector, and {Ü} is the acceleration vector.

2.2 Natural frequencies model

Natural frequencies are giving the resonant frequencies of the system and it is very important indicative of dynamic behavior.

Removing external loads, the equations of the system become:

$$[M]\{\ddot{U}\}+[K]\{U\}=0 \quad (3)$$

Considering solution as harmonic vibration:

$$\{U\}=\{X\}\sin(\omega t) \quad (4)$$

where, {*X*}is displacement amplitude, *ω* is rotational frequency, *t* is time, the equations of motion become:

$$[K]\{X\}=\omega^2[M]\{X\} \quad (5)$$

Before solution is necessary to reduce to standard form [12]

$$[A]\{Z\}=\omega^2\{Z\} \quad (6)$$

where [A] is symmetric, [Z] represents the eigenvector and ω2 the eigenvalue. There are several algorithms to solve the equations. Among them, Inverse Iteration Method, Jacobi, Lanczos, or Arnoldi are most used. FEMCAS implements the Jacobi algorithm for modal analysis [12].

2.3 Deterministic dynamic model

This module completes the deterministic linear analysis module and analyze linear systems under dynamic loads. This program can be used also for static analysis. The static analysis is a quasi-static where the time is applied slow over the amplitude to reduce the kinetic energy. In quasi-static analysis the kinetic energy should be minimized.

Consider equation of motion in matrix form:

$$[M]\{\ddot{U}\}+[C]\{\dot{U}\}+[K]\{U\}=\{F\} \quad (7)$$

where, [M] is the mass matrix, [C] is the damping matrix, [K] is the stiffness matrix, {F} is external applied force vector, {U} is the displacement vector, {U̇} is the velocity vector and {Ü} is the acceleration vector. The system is solved by finite element method and the results are displacement, velocity, and acceleration. The equation of motion includes this time the damping therm.

The program is made in Fortran and calculates the displacement of beam elements type under time dependent external forces [12]. The algorithm is using the Newmark direct method which involves the use of time parameters and . The values of these parameters determine the accuracy and stability of the algorithm. By default, FEMCAS uses β=0.25 and γ=0.5.

It starts from initial state of the bar model were, according to known material data is calculating the initial mass matrix $[M]_0$, initial damping matrix $[C]_0$ and initial stiffness matrix $[K]_0$. The initial conditions of the system $\{U\}_0$ and {U̇}0 are also known.

2.4 Uncertainty dynamic model

Degradation of stiffness parameters is an aspect that is not considered by current simulations, which consider the model to be geometrically and materially perfect. This is not the case in physical models because they include imperfections in fabrication and operation. These imperfections can be quantified using statistical computation and modelled as uncertainties. Geometrical and material uncertainty is considered for bending stiffness parameters. The bending stiffness parameters can be modeled as $EI=\overline{EI}+\widetilde{EI}$. E is the modulus of elasticity (material property), I is the moment of inertia of the cross-section of the beam (geometrical property). The mean values $\overline{EI}$ are assumed to be much larger than the root mean square of the variability of the random field represented by $\widetilde{EI}$. The random field is assumed to be Gaussian distributed with zero mean having standard deviation, σ_{EI}, much smaller than the corresponding mean value. This implies that the stiffness parameters form random fields with positive value.

2.4.1 Monte Carlo model

Monte Carlo simulation consists in the numerical accumulation of a population corresponding to the random quantities in the physical problem, solving the problem associated with each member of the respective population and obtaining a population corresponding to the random response quantities. This population can then be used to obtain the statistics of the response variables.

To include uncertainties, random fields will be generated for each finite element and assembled in the general matrix. Monte Carlo simulation consists of solving the equations of motion, which includes random variables divided by elements, several times. The higher the number of solvers, the higher the accuracy is. A minimum of 1000 runs is required for acceptable accuracy. This is computational expensive, especially if the simulation models will be large (high nodes and elements). This method has a high accuracy compared to other stochastic calculation methods.

2.4.2 Perturbation method

The perturbation method applied in finite element analysis is known in the literature as PFEM (Probabilistic Finite Element Method). We consider the equation of motion in matrix form:

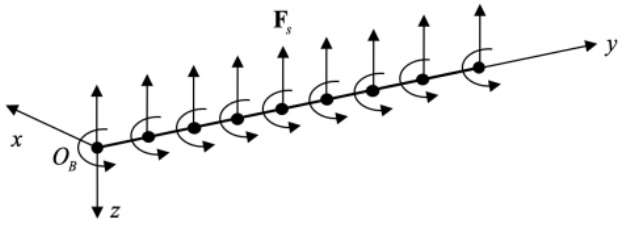

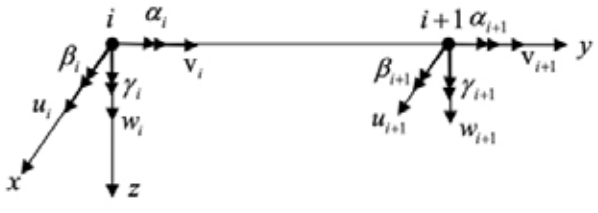

Fig. 2. (a)Finite Element Discretization. (b)One Finite Element. [10]

$$[M]\{\ddot{U}\}+[C]\{\dot{U}\}+[K]\{U\}=\{F\} \quad (8)$$

where, [M] is the mass matrix, [C] is the damping matrix, [K] is the stiffness matrix, {F} is the applied external force vector, {U} is the displacement vector, $\{\dot{U}\}$ is the velocity vector and $\{\ddot{U}\}$ is the acceleration vector. Geometrical and material uncertainty is considered for bending stiffness parameters. The bending stiffness parameters are shown below:

$$EI=\overline{EI}+\widetilde{EI} \quad (9)$$

Where E is the modulus of elasticity (material property), I is the moment of inertia of the cross-section of the beam (geometrical property). The mean values $\overline{EI}$, are assumed to be much larger than the root me an square of the variability of the random field represented by $\widetilde{EI}$. The random field is assumed to be Gaussian distributed with zero mean, with the standard deviation σ_{EI} being much smaller than the corresponding mean value.This implies that the stiffness parameters form random fields with positive value.

Returning to the equation of motion (8), the stiffness matrix , includes the bending stiffness parameters . The degradation of stiffness parameters can be quantified using equation (9).In finite element analysis, the stiffness matrix includes values split into elements and nodes. To include uncertainties, random fields will be generated for each individual element which will be introduced into the overall matrix. Mass, damping, and external forces are considered deterministic.

The perturbation method involves Taylor series extension of the stiffness matrix and is a numerically less expensive alternative to the Monte Carlo method.

In mathematics, a Taylor series is a representation of a function as an infinite sum of terms computed from the derivative values of that function at a point. The stiffness matrix can be represented in Taylor series according to the relation [8]:

$$K=K_0+\sum_{i=1}^{N} K_i^{I}a_i+\frac{1}{2}\sum_{i=1}^{N}\sum_{j=1}^{N} K_{ij}^{II}a_ia_j+\dots \quad (10)$$

where K_0 is the mean of matrix K, K_i^{I} is the first partial derivative of K with respect to the random variable a_i, K_{ij}^{II} is the second partial derivative of K with respect to the random variables a_i and a_j evaluated at {a}=0:

$$K_i^{I}=\left.\frac{\partial K}{\partial a_i}\right|_{\{a\}=0};\quad K_{ij}^{II}=\left.\frac{\partial K}{\partial a_i\partial a_j}\right|_{\{a\}=0} \quad (11)$$

To solve equation (8), it is also necessary to represent the displacement, velocity, and acceleration vector in Taylor series:

$$U=U_0+\sum_{i=1}^{N} U_i^{I}a_i+\frac{1}{2}\sum_{i=1}^{N}\sum_{j=1}^{N} U_{ij}^{II}a_ia_j+\dots \quad (12.1)$$

$$\dot{U}=\dot{U}_0+\sum_{i=1}^{N} \dot{U}_i^{I}a_i+\frac{1}{2}\sum_{i=1}^{N}\sum_{j=1}^{N} \dot{U}_{ij}^{II}a_ia_j+\dots \quad (12.2)$$

$$\ddot{U}=\ddot{U}_0+\sum_{i=1}^{N} \ddot{U}_i^{I}a_i+\frac{1}{2}\sum_{i=1}^{N}\sum_{j=1}^{N} \ddot{U}_{ij}^{II}a_ia_j+\dots \quad (12.3)$$

where U_0, $\dot{U}_0$,$\ddot{U}_0$ are the mean values and U_i^{I}, $\dot{U}_i^{I}$, $\ddot{U}_i^{I}$, U_{ij}^{II}, $\dot{U}_{ij}^{II}$, $\ddot{U}_{ij}^{II}$ are the first and second derivatives of the random variables a_i and a_j, evaluated at {a}=0.

Considering the Taylor series representation up to order 1, the displacement, velocity and acceleration vectors are obtained by successive solvers as follows:

0-order equations:

$$M\ddot{U}_0+C\dot{U}_0+K_0U_0=F \quad (13.1)$$

First order equations:

$$M\ddot{U}_i^{I}+C\dot{U}_i^{I}+K_0U_i^{I}=-K_i^{I}U_0 \quad (13.2)$$

Statistical values using the first order approximation are calculated as follows:

Mean value:

$$E[U]=U_0 \quad (14.1)$$

$$E[\dot{U}]=\dot{U}_0 \quad (14.2)$$

$$E[\ddot{U}]=\ddot{U}_0 \quad (14.3)$$

Covariance:

$$COV(U,U)=E\left\{[U-E[U]][U-E[U]]^T\right\}=\sum_i^N\sum_i^N U_i^{I}(U_i^{I})^T E[a_ia_i] \quad (15.1)$$

$$COV(\dot{U},\dot{U})=E\left\{\left[\dot{U}-E[\dot{U}]\right]\left[\dot{U}-E[\dot{U}]\right]^T\right\}=\sum_i^N\sum_i^N \dot{U}_i^{I}(\dot{U}_i^{I})^T E[a_ia_i] \quad (15.2)$$

$$COV(\ddot{U},\ddot{U})=E\left\{\left[\ddot{U}-E[\ddot{U}]\right]\left[\ddot{U}-E[\ddot{U}]\right]^T\right\}=\sum_i^N\sum_i^N \ddot{U}_i^{I}(\ddot{U}_i^{I})^T E[a_ia_i] \quad (15.3)$$

Variance:

$$Var[U,U]=diag[COV(U,U)]=\sum_i^N\sum_i^N diag\left[U_i^{I}(U_i^{I})^T\right]E[a_ia_i] \quad (16.1)$$

$$Var[\dot{U},\dot{U}]=diag[COV(\dot{U},\dot{U})]=\sum_i^N\sum_i^N diag\left[\dot{U}_i^{I}(\dot{U}_i^{I})^T\right]E[a_ia_i] \quad (16.2)$$

$$Var[\ddot{U},\ddot{U}]=diag[COV(\ddot{U},\ddot{U})]=\sum_i^N\sum_i^N diag\left[\ddot{U}_i^{I}(\ddot{U}_i^{I})^T\right]E[a_ia_i] \quad (16.3)$$

2.4.3 Neumann method

The Neumann method applied in finite element analysis is known in the literature as SSFEM (Spectral Stochastic Finite Element Method) [9]. Uncertainties are modeled using a modified first-order stochastic perturbation method together with a truncated Karhunen-Loeve expansion instead of the Taylor series [10]. The Taylor series is used only for the displacement vector expansion. The Neumann method involves the Karhunen-Loeve (K-L) series extension of the stiffness matrix and is a numerically less expensive alternative to the Monte Carlo method, with higher accuracy than the perturbation method. The continuous random field model will be discretized using the Karhunen-Loeve (K-L) series. Geometric and material uncertainty is considered for the bending stiffness parameters. The bending stiffness parameters are shown below [10]:

$$EI_x(y,\theta)=\overline{EI_x}+\sum_{r=1}^{NKL}\sqrt{\lambda_r}f_r(y)a_r(\theta) \quad (17)$$

where $a_r(\theta)$ are orthonormal random variables of mean 0 with θ belonging to the space of random events; NKL is the number of K-L series; f, λ_i are functions and eigenvalues of the covariance $C(y_1,y_2)$ [8, 9]:

$$\int_{-L/2}^{L/2} C(y_1,y)f(y_1)dy_1=\lambda f(y) \quad (18)$$

where $C(y,y_1)=\sigma_{EI_x}^2 e^{-|y-y_1|/l_{cor}}$, L is the length of the bar, l_{cor} l_{cor} is the correlation length, l_{cor} / L = 1, y,y1∈[-L/2, L/2], $\sigma_{EI_x}^2$ is the variance of the random field.

Equation (18) can be solved analytically for the one-dimensional case [4, 5]. Equation (18) can be written as:

$$\int_{-L/2}^{y}\sigma_{EI_x}^2 e^{-(y-y_1)/l_{cor}}f(y_1)dy_1+\int_{y}^{L/2}\sigma_{EI_x}^2 e^{(y-y_1)/l_{cor}}f(y_1)dy_1=\lambda f(y) \quad (19)$$

Differentiate equation (19) in y, we obtain:

$$-\frac{\sigma_{EI_x}^2}{l_{cor}}\int_{-L/2}^{y} e^{-(y-y_1)/l_{cor}}f(y_1)dy_1+\frac{\sigma_{EI_x}^2}{l_{cor}}\int_{y}^{L/2} e^{(y-y_1)/l_{cor}}f(y_1)dy_1=\lambda f'(y) \quad (20)$$

Differentiate equation (20) in y, we obtain:

$$\lambda_i f''(y)+\left(2\frac{1}{l_{cor}}\sigma_{EI_x}^2-\frac{1}{l_{cor}^2}\lambda_i\right)f_i(y)=0 \quad (21)$$

By introducing

$$\omega^2=\left(2\frac{\sigma_{EI_x}^2}{l_{cor}}-\frac{1}{l_{cor}^2}\lambda\right)\frac{1}{\lambda} \quad (22)$$

equation (20) becomes:

$$f''(y)+\omega^2 f(y)=0 \quad (23)$$

Evaluating equations (18) and (19) at y=-L/2 and y=L/2, the boundary conditions for equation (23) are obtained as follows:

$$\frac{1}{l_{cor}}f(L/2)+f'(L/2)=0 \quad (24.a)$$

$$\frac{1}{l_{cor}}f(-L/2)-f'(-L/2)=0 \quad (24.b)$$

The solution of equation (23) is:

$$f(y)=a_1\cos(\omega y)+a_2\sin(\omega y) \quad (25)$$

From equation (25) and (23) by applying boundary conditions (17) yields the following equations:

$$a_1\left(\frac{1}{l_{cor}}-\omega\tan\left(\omega\frac{L}{2}\right)\right)+a_2\left(\omega+\frac{1}{l_{cor}}\tan\left(\omega\frac{L}{2}\right)\right)=0 \quad (26.a)$$

$$a_2\left(\frac{1}{l_{cor}}-\omega\tan\left(\omega\frac{L}{2}\right)\right)-a_2\left(\omega+\frac{1}{l_{cor}}\tan\left(\omega\frac{L}{2}\right)\right)=0 \quad (26.b)$$

Considering the zero determinant gives the following transcendental equations:

Table 1 – Natural frequency results comparison

Mode No	Frequency (Hz)		
	Solid 3D Adams [11]	Abaqus	FEMCAS
1	1335.5	1334.4	1338
2	1335.5	1334.4	1338
3	3413	3444.5	3458
4	3413	3444.5	3458
5	5811	6427	6436
6	5811	6427	6436

Table 2 – Simulation time

	Monte Carlo	Perturbation	Neumann
Simulation Time (s)	840.2	5.34	51.1

$$\frac{1}{l_{cor}} - \omega\tan\left(\omega\frac{L}{2}\right) = 0;\quad \omega + \frac{1}{l_{cor}}\tan\left(\omega\frac{L}{2}\right) = 0 \tag{27.a,b}$$

Noting the solution of equation (27.b) by ω*, the eigen functions are:

$$f_r(y)=\frac{\cos(\omega_r y)}{\sqrt{\frac{L}{2}+\frac{\sin(2\omega_r L/2)}{2\omega_r}}}\ ;\ f_r^*(y)=\frac{\sin(\omega_r^* y)}{\sqrt{\frac{L}{2}-\frac{\sin(2\omega_r^* L/2)}{2\omega_r^*}}} \tag{28.a,b}$$

for even and odd values of r respectively. The corresponding eigen values are:

$$\lambda_r=\frac{2\sigma_{E_0}^2 l_{cor}}{\omega_r^2+1/l_{cor}^2}\quad ;\quad \lambda_r^*=\frac{2\sigma_{E_0}^2 l_{cor}}{\omega_r^{*2}+1/l_{cor}^2} \tag{29.a,b}$$

for even and odd values of r respectively.

By inserting equation (17) into the expression for elementary stiffness, the following expression is obtained:

$$K_e(\theta)=EI_z\left(\int_{y_i}^{y_{i+1}} N_w''(y)^T N_w''(y)dy\right)+AE\left(\int_{y_i}^{y_{i+1}} N_v'(y)^T N_v'(y)dy\right)+\overline{EI_x}\left(\int_{y_i}^{y_{i+1}} N_w''(y)^T N_w''(y)dy\right)+$$
$$\int_{y_i}^{y_{i+1}}\sum_{r=1}^{NKL}\sqrt{\lambda_r}f_r(y)a_r(\theta)\,N_w''(y)^T N_w''(y)dy+GJ\left(\int_{y_i}^{y_{i+1}} N_\alpha'(y)^T N_\alpha'(y)dy\right) \tag{30}$$

Where ' denotes the first derivative, '' denotes the second derivative, A is the cross-sectional area, E is the modulus of elasticity, G is the shear modulus, I moments of inertia on different axes (u-perpendicular direction, v axial direction, w vertical direction), J is the torsional modulus,

$N_u = [N_3\ 0\ 0\ 0\ 0\ N_5\ N_4\ 0\ 0\ 0\ 0\ N_6]$

$N_v = [0\ N_1\ 0\ 0\ 0\ 0\ 0\ N_2\ 0\ 0\ 0\ 0]$

$N_w = [0\ 0\ N_3\ N_5\ 0\ 0\ 0\ 0\ N_4\ N_6\ 0\ 0]$

$N_\alpha = [0\ 0\ 0\ 0\ N_1\ 0\ 0\ 0\ 0\ 0\ N_2\ 0]$

are the shape function vectors:

$$N_1=\frac{y_{i+1}-y}{y_{i+1}-y_i},\ N_2=\frac{y-y_i}{y_{i+1}-y_i},\ N_3=1-3\left(\frac{y-y_i}{y_{i+1}-y_i}\right)^2+2\left(\frac{y-y_i}{y_{i+1}-y_i}\right)^3,\ N_4=3\left(\frac{y-y_i}{y_{i+1}-y_i}\right)^2-2\left(\frac{y-y_i}{y_{i+1}-y_i}\right)^3,\ N_5=(y-y_i)-\frac{2}{y_{i+1}-y_i}(y-y_i)^2+$$
$$\frac{1}{(y_{i+1}-y_i)^2}(y-y_i)^3,\ N_6=-\frac{1}{y_{i+1}-y_i}(y-y_i)^2+\frac{1}{(y_{i+1}-y_i)^2}(y-y_i)^3,\ y_i\le y\le y_{i+1}.$$

The notation below is made:

$$K_{e,r}=\int_{y_i}^{y_{i+1}}\sqrt{\lambda_r}f_r(y)N_w''(y)^T N_w''(y)dy$$

and

$$K_{e0}=EI_z\left(\int_{y_i}^{y_{i+1}} N_w''(y)^T N_w''(y)dy\right)+AE\left(\int_{y_i}^{y_{i+1}} N_v'(y)^T N_v'(y)dy\right)+\overline{EI_x}\left(\int_{y_i}^{y_{i+1}} N_w''(y)^T N_w''(y)dy\right)+GJ\left(\int_{y_i}^{y_{i+1}} N_\alpha'(y)^T N_\alpha'(y)dy\right)$$

The elementary matrix becomes:

$$K_e(\theta)=K_{e0}+\sum_{r=1}^{NKL}K_{e,r}a_r(\theta) \tag{31}$$

Putting the element matrices together we get the global equation:

$$M\ddot{U}(t,\theta)+C\dot{U}(t,\theta)+K_0U(t,\theta)+\left(\sum_{r=1}^{NKL}K_{e,r}a_r(\theta)\right)U(t,\theta)=F(t) \tag{32}$$

where F is the vector of external forces.

Applying the first-order perturbation method the displacement vector is represented in Taylor of order one:

$$U=U_0+\sum_{i=1}^{NKL}U_i^I a_i \tag{33.1}$$
$$\dot{U}=\dot{U}_0+\sum_{i=1}^{NKL}\dot{U}_i^I a_i \tag{33.2}$$
$$\ddot{U}=\ddot{U}_0+\sum_{i=1}^{NKL}\ddot{U}_i^I a_i \tag{33.3}$$

where U_0, $\dot{U}_0$,$\ddot{U}_0$ are mean values, and U_i^I, $\dot{U}_i^I$, $\ddot{U}_i^I$, the first derivative relating to the random variable a_i evaluated at {a}=0.

Considering the Taylor series representation up to order 1, the displacement, velocity and acceleration vectors are obtained by successive solvers as follows:

0-order equations:

$$M\ddot{U}_0+C\dot{U}_0+K_0U_0=F \tag{34.1}$$

First-order equations:

$$M\ddot{U}_i^I+C\dot{U}_i^I+K_0U_i^I=-K_i^IU_0 \tag{34.2}$$

Statistical values using the first order approximation are calculated as follows:

Mean value:

$$E[U]=U_0 \tag{35.1}$$
$$E[\dot{U}]=\dot{U}_0 \tag{35.2}$$
$$E[\ddot{U}]=\ddot{U}_0 \tag{35.3}$$

Covariance:

$$COV(U,U)=E\left\{[U-E[U]][U-E[U]]^T\right\}=\sum_i^{NKL}\sum_i^{NKL}U_i^I(U_i^I)^T E[a_ia_i] \tag{36.1}$$
$$COV(\dot{U},\dot{U})=E\left\{\left[\dot{U}-E[\dot{U}]\right]\left[\dot{U}-E[\dot{U}]\right]^T\right\}=\sum_i^{NKL}\sum_i^{NKL}\dot{U}_i^I(\dot{U}_i^I)^T E[a_ia_i] \tag{36.2}$$
$$COV(\ddot{U},\ddot{U})=E\left\{\left[\ddot{U}-E[\ddot{U}]\right]\left[\ddot{U}-E[\ddot{U}]\right]^T\right\}=\sum_i^{NKL}\sum_i^{NKL}\ddot{U}_i^I(\ddot{U}_i^I)^T E[a_ia_i] \tag{36.3}$$

Variance:

$$Var[U,U]=diag[COV(U,U)]=\sum_i^{NKL}\sum_i^{NKL}diag\left[U_i^I(U_i^I)^T\right]E[a_ia_i] \tag{37.1}$$
$$Var[\dot{U},\dot{U}]=diag[COV(\dot{U},\dot{U})]=\sum_i^{NKL}\sum_i^{NKL}diag\left[\dot{U}_i^I(\dot{U}_i^I)^T\right]E[a_ia_i] \tag{37.2}$$
$$Var[\ddot{U},\ddot{U}]=diag[COV(\ddot{U},\ddot{U})]=\sum_i^{NKL}\sum_i^{NKL}diag\left[\ddot{U}_i^I(\ddot{U}_i^I)^T\right]E[a_ia_i] \tag{37.3}$$

3. SIMULATION

3.1 Modal Analysis

The geometric model in Figure 1 was analyzed with the commercial FEA program Abaqus[13] and a new FEA program called FEMCAS [14]. In Abaqus the structure was modelled with BEAM elements. In FEMCAS the structure was modelled with beam type elements. The model tested is an unconstrained beam.

The table below show a comparison of the results.

We notice that our own modes correlate very well at low frequencies. At high frequencies, the discrepancies between the analyzes begin to

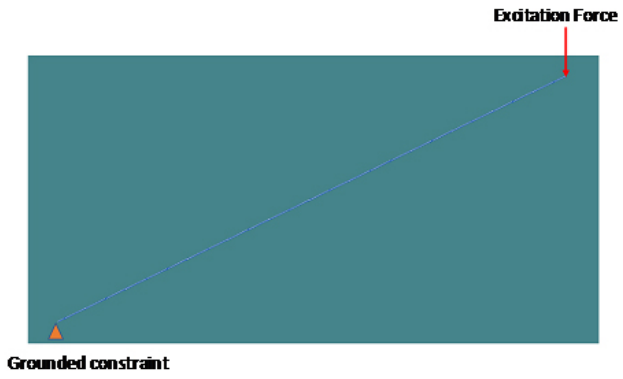

Fig. 3. Boundary conditions and loads

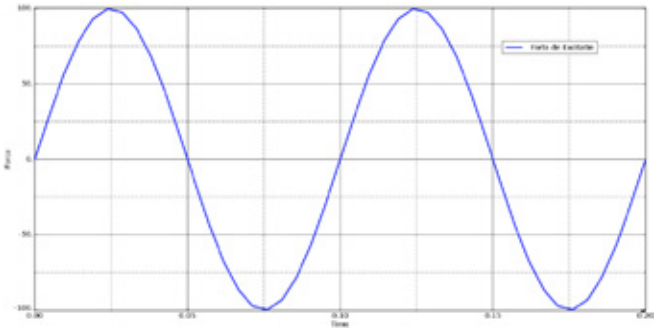

Fig. 4. Time history of excitation force

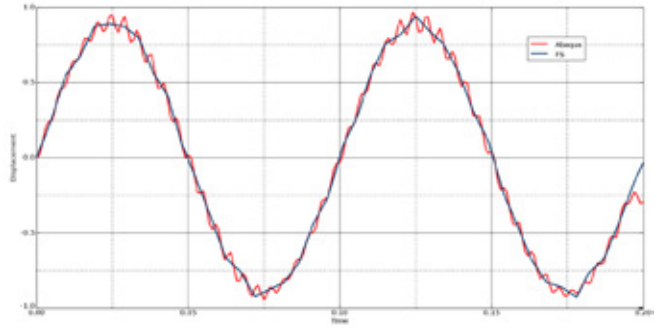

Fig. 5. Vertical displacement response history at the bar end where the force is exerted.

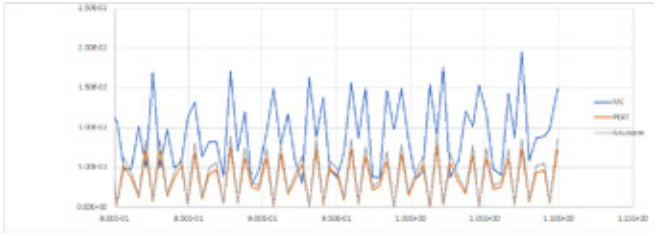

Fig. 6. Standard deviation of the vertically displacement response

increase. The difference between the solid 3D model in Adams and the models in Abaqus and FEMCAS is due to the simplification of the 3D model into the bar model. We notice very good correlation between Abaqus and FEMCAS models.

3.2 Dynamic Analysis

The geometric model in Figure 1 is subjected to a forced vibration. The bar is constrained at one end and at the other is subjected to a force of harmonic excitation (see Figure 3) in a vertical direction.

Time history of excitation force is shown in figure 4.

The analysis was carried out in FEMCAS and Abaqus and the result is shown in Figure 5.

We observe a good correlation between Abaqus and FEMCAS which gives confidence and accuracy to the developed program.

3.3 Dynamic Analysis with parametric uncertainties

Uncertainties are introduced into the vertical rigidity matrix. A field of random variables with Gaussian distribution with zero mean and standard deviation 0.01 is generated. The results shown in Figure 6 represent the standard deviation of the displacement at the point of application of the force in the vertical direction. We see a good correlation between the disturbance and Neumann. In this case the Monte Carlo method has a higher standard deviation.

The analysis time is greatly improved in the case of the perturbation methods and Neumann as presented in Table 2.

5. CONCLUSION

Following the tests carried out, the FEMCAS software proposed is robust, reliable, fast and has good accuracy. It is an additional step in the analysis with finite elements that includes the influence of uncertainties. The inclusion of uncertainties increases the robustness and reliability of the product resulting from the design.

REFERENCES:

[1] Fissore, D, *Robust control in presence of parametric uncertainties: observer based feedback controller design*. Chemical Engineering Science (Elsevier), 63(7), 1890-1900 (2008)

[2] Williamson D. B., Blaker T.A, Sinha B., *Tuning without over-tuning: parametric uncertainty quantification for the NEMO ocean model*, Geosci. Model Dev., 10, 1789–1816 (2017)

[3] Hebeler, F., Ross S. Purves, Stewart S.R. Jamieson, *The impact of parametric uncertainty and topographic error in ice-sheet modelling*, Journal of Glaciology, Volume 54, Issue 188, University of Lethbridge, Canada (2017)

[4] Pascal Brault, Quentin Delamare, Paolo Robuffo Giordano. *Robust Trajectory Planning with Parametric Uncertainties*. ICRA 2021 - IEEE International Conference on Robotics and Automation, May 2021, Xi'an, China. pp.11095-11101. ffhal-03260768f

[5] Jana Závacká, Monika Bakošová, KatarínaVaneková, *Control of systems with parametric uncertainties using a robust PI controller*, AT&P journal PLUS2 (2007)

[6] Karim Lenhard, *Determination of combined measurement uncertainty via Monte Carlo analysis for the imaging spectrometer ROSIS*, Applied Optics Vol. 51, Issue 18, pp. 4065-4072 (2012)

[7] Scardigli, F., *The deformation parameter of the generalized uncertainty principle*, 9th International Workshop DICE : Spacetime - Matter - Quantum Mechanics (2018)

[8] Papadopoulos, V., Giovanis, D.g., *Stochastic Finite Element Methods: An Introduction*, Springer-Verlag Switzerland (2018)

[9] Ghanem, G.G. and Spanos, P.D., *Stochastic finite elements: A spectral approach*, Springer-Verlag New York (1991)

[10] Castravete, Stefan, *Nonlinear flutter of a cantilever wing including the influence of structure uncertainties*, ProQuest Dissertations Publishing, 3295976 (2007).

[11] Marinescu, G.C., *Contribuții la analiza unor mecanisme de direcție, cu considerarea elementelor deformabile*, Teza de doctorat, Universitatea din Craiova, Facultatea de Mecanică, Craiova, (2012).

[12] Margetts, L., Smith, I. M., & Griffiths, D. V, *Programming the Finite Element Method. (5th ed.)*, John Wiley & Sons Ltd.2014

[13] Dassault Systemes, Simulia Abaqus 2021 documentation, Dassault Systemes. 2021

[14] Fluid Struct, FEMCAS Documentation, Fluid Struct. 2022

THE STUDY OF THE SUN VISOR INFLUENCE OVER THE DRIVER'S VIEW USING THE CAVE AT THE INTERIOR DESIGN PHASE

STUDIUL INFLUENȚEI PARASOLARULUI ASUPRA CÂMPULUI VIZUAL AL ŞOFERULUI UTILIZÂND SISTEME DE SIMULARE A REALITĂȚII VIRTUALE ÎN FAZA DE DESIGN INTERIOR

REZUMAT: *Pentru creşterea productivităţii se caută soluţii de optimizare a ciclului de viaţă în orice domeniu. Pentru aceasta o data cu digitalizarea sistemelor s-a dezvoltat şi prototiparea virtuală. Dacă iniţial a fost una 2D la care imaginile erau analizate pe ecrane mari, acum pe scară largă se implementează tehnologia de prototipare 3D tip CAVE. Articolul îşi propune să prezinte pe scurt procesul de verificare a comptabilităţii unui parasolar cu configuraţia interioară a unui autovehicul. Acest lucru trebuie să ţină cont de factori constructivi ai autovehiculului (tipul şi poziţia prinderilor etc.) dar şi de influenţele pe care le poate avea asupra câmpului vizual pentru diferite tipuri de clienţi (pe clase de mărime). Este necesar acest lucru pentru a satisface cerinţe legate de ergonomicitate şi siguranţă în utilizare. Compatibilitatea putea fi verificată prin scheme 2D sau prin comandarea şi montarea fizică a unui prototip în vederea observării acestuia. Acest lucru implică cheltuieli sporite şi timp mai mare de validare. În ceea ce priveşte ciclul de viaţă, acesta ar avea mai multe iteraţii ce pot duce la întârzieri la apariţia produsului finit.*
Keywords: *CAVE, Virtual Prototyping, Digital Mock-Up, Life Cycle, Sun Visor.*

S. l. dr. ing.
Ștefan VOLOACĂ[1]
stefan.voloaca@upb.com

Drd. ing.
Anca-Alexandra IORDACHE SABO[2]

[1] Universitatea POLITEHNICA din București, Spl. Independenței, Nr. 313, 060042 BUCUREȘTI, România
[2] Renault Technologie Roumanie S.R.L., Str. Preciziei, Nr. 3G, BUCUREȘTI, România

1. INTRODUCTION

In any industry the main development element is the speed of acting to satisfy the client's needs. This thing meets a tight collaboration between vast domains. A small example is represented by the mechatronic domain that helped developing all the domains combining mechanics and electronics.

Since 1992, when the CAVE (Audio Visual Experience Automatic Virtual Environment) was first presented as a virtual reality interface [1], the use of it rises fast in many domains.

The virtual reality (VR) creates an alternate reality that the user can experience without input from the real life, so the whole experience is digitally controlled [2], while the augmented reality (AR) combines the physical world with the digital content.

Three of the main applications of virtual reality (VR) that present valuable opportunities for product development, in general, are: simulation, skills training, and communication [3]. This way, using virtual reality (VR) was possible to develop a new branch in the product life cycle management (PLM) like virtual prototyping (VP). The CAVE is an interactive tool used to develop new products especially with their increasing product complexity. They can be beneficial in many aspects like product quality, time-to-market, and cost competitiveness [4].

It can be used in a vast domain of research and education like Civil Engineering, Architecture, Automotive, Aeronautics or Naval [5][6][7].

A main use of the CAVE, in the interior design, is the study of the vehicle ergonomics. Regardless of the domain, aeronautic or automotive it is possible to check if the vehicle conforms to safety requirements, analyze reachability and accessibility, check ergonomics of the onboard computer and enhance the creative process: personalize a vehicle by changing the dashboard, options or rearview mirrors [8].

The quality of the images is at a high resolution and clarity including real environment light density. It is adapted for different materials, including the LCD multimedia displays [9].

With a fast response, it can be used as a pilot simulator in the automotive industry [5] or even in the aeronautic one [10].

In the automotive industry the final product is obtained by a long time-consuming chain of iterations between fields of design, simulation, and validation. Creating a virtual prototype, named Digital Mock-Up helped in reducing the number of long iterations. To shorten the product development time, design evaluations must be done faster, the results must be directly incorporated into the design process [11].

This Mock-Up represents an assembly of virtual components obtained using Computer Aided Design in different locations over the world. It plays an important role in the communication of product information among a variety of users, including marketing people, customers, managers, product development teams and engineering and even repair and maintenance people [12].

2. INTERIOR DESIGN

2.1 Internal or international standardization

In the phase of the interior design, one of the most critical analyzed elements is represented by the eyellipse.

The eyellipse represents the contraction of the words "eye" and "ellipse" used to describe a statistically derived elliptical model representing driver eye locations in road vehicles [13].

Starting from the studies made on the drivers, it was possible to determine their eyes' position. The position is determined when the driver sits on the seat at a back angle between 5 to 40 degrees. In the lateral view those positions determine the eyellipse. The eyellipse determination was made in 50/50 parts of a gender mix. An eyellipse of 95% do not represents the position of the 95% of the people's eyes are inside the ellipse. Seeing from the lateral, a tangent plane to the upper side of the ellipse will have 95% of the eyes below that line and 5% above it. But if the plane will be tangent to the lower part of the ellipse 95% of the population's eyes will be above and 5% below.

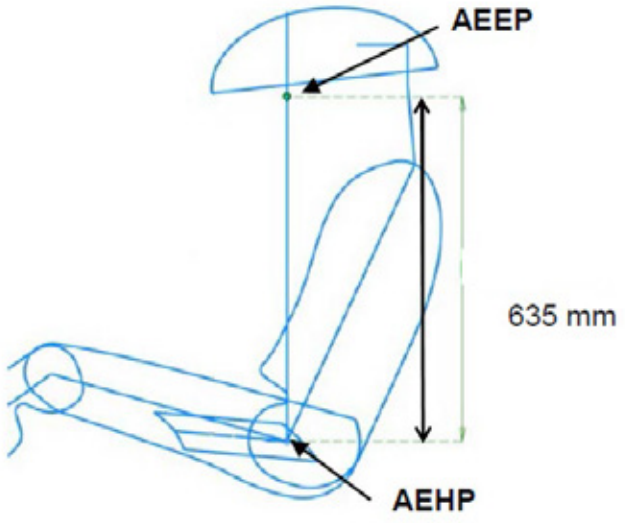

Fig. 1. The driver's coordinate position

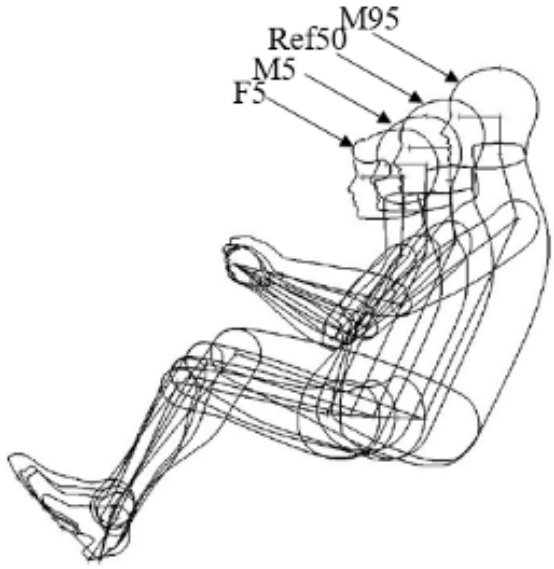

Fig. 2. The main types of the dummies

Every car manufacturer can use the international standard or can create its own internal standards. To increase the analyze efficiency, The Renault-Nissan Group simplified the position by defining the Eye Point position (AEEP - Alliance Exchange Eye Point). It is situated at a height of 635mm on the vertical direction above the Hip Point (AEHP – Alliance Exchange Hip Point) (Figure 1).

When designing a cabin, especially the driving place is necessary to position the main elements like the driving seat, steering wheel etc. Their position must be adjustable to be easily used no matter the size or gender of the user. This way classes were created by the people size or gender (Figure 2). Those classes show the percentage of people that fits in.

When an element like the crank cannot be adjusted the gender class is used due to the specific clothes and shoes characteristics.

Every class has a dummy that has dimensions representative of that class. The F5 dummy represents 5% of Females while M5 are 5% of Males. Half of the population, no matter the gender, is represented by the Ref50 dummy. The tall people are represented by M95.

2.2 The CAVE

Nowadays it is easy to work on the interior design by using a CAVE. The CAVE is situated inside the Renault research center in Titu, Dâmbovița district. It has five active walls (including the floor), on which the images are projected from ten Barco 4K video-projectors. The 3D image is created by two projectors for every wall. Their light is reflected through high reflective mirrors. Using 3D glasses, with infrared sensors, is possible to perceive a realistic image of the designed model at a normal scale. For good observation, the user can walk through the room or use a fly stick as a controller, to move the virtual model.

Every designer can upload a part of the prototype developed in CATIA. The components are assembled in a Digital Mock-Up that can be visualized on a wide high-quality display (84"), in a 2D format, or in a 3D format inside the CAVE.

By introducing different material characteristics, like texture, color etc. the image will look realistic. To project this realistic image every projector has its own computer. Thus, it is easy to maneuver the image for a good observation.

The processing computers are Hewlett Packard type Z8 with 64GB of RAM, Intel Xeon Gold 5120 CPU @ 2.20 GHz (28 CPUs) processor and Nvidia P6000 graphical card.

Initially the designed parts in CATIA have 9 GB together. They must be put together and bring to a satisfying resolution of 4096x2160 pixels. This way the image quality makes possible the observation of images up to 20cm distance. The resulting dimension of the Mock-Up will be around 1.3 GB, facilitating a fast maneuvering of the 3D model.

2.3 The real use of the CAVE

The sun visor was first patented in the year 1938 under the name Glare Shield [14]. Since then, its principle was to protect the driver against the dazzle present in the evening and morning hours and when the hills are climbed [15]. Over the years it had different geometries or functions. Some of them could have adjustable extensions. With the current tendencies the sun visors could be automated. An automatic sun visor system, for a vehicle, includes a light detecting apparatus for detecting sunlight incident upon the face of an occupant of the vehicle [16]. The adjustable sun visor will change its darkness corresponding to the detected sunlight. New ideas offer revolutionary Virtual Visor, a transparent LCD and intuitive camera, which replaces the traditional vehicle sun visor completely [17].

To produce and implement an automated sun visor on a day-by-day vehicle will bring higher costs and technology. That is why the classical one will be used on most of the vehicles and should study its fit in the interior design using CAVE.

When designing a sun visor, it starts from a specified dimension (length x height). If the coordinates are in the boundary box, the next check will be if the sun visor satisfies sun shading and visibility requirements. There will be some results. If they satisfy the rules they will pass to the management and standardization team that will send the dimensions for the detailed design of the sun visor.

If the results are not quite good, they will have to make design changes with the vehicle project team to control roof layout for an acceptable fitting position.

Even if the dimensions are in the internal standardization map, the

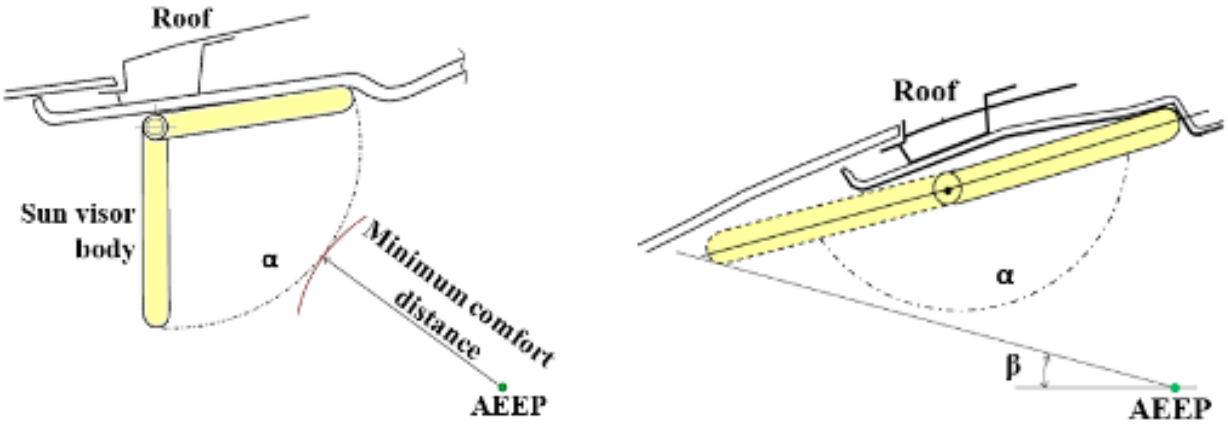

Fig. 3 Lateral view of the different position angles of the sun visor (left – α=120°, right – α=170°)

analysis of the visibility must be made for three positions of the sun visor. The first will be for the folded position and the next two for 120 and 170 degrees (Figure 3).

The benefit of the CAVE is represented by its produced results. They can be subjective results or objective results.

The subjective results can be analyzed directly on the screen by the engineer, everywhere in the world. The objective results are the realistic results, where the images are realistic and can be directly observed. This way it is possible to easily estimate any imperfections and fix them quickly.

3. RESULTS AND INTERPRETATION

3.1 Subjective results

With the CAVE is possible to generate images for different types of standardized drivers. The study was made for different markets by analyzing eyellipse that fits in different percentage of men or women.

With the CAVE were created images special for the studied classes. The image is presented from the eyes of a dummy that represents the studied class. Its eyes are positioned at a specific coordinate according to international or internal standards. For all types of dummies, there are generated figures that have three images. The first one is for the folded sun visor, second one for a position of 120 degrees, that represents the adverse situation, and the third one for a 170 degree.

For good observation, the front windshield is divided in equal parts by 10 horizontal lines. The lines have different colors depending on their relevance.

When driving at high speed the driver will focus up to the horizon line. That line will be represented with green. The critical line of the windshield

Fig. 4. Driver's view - F5

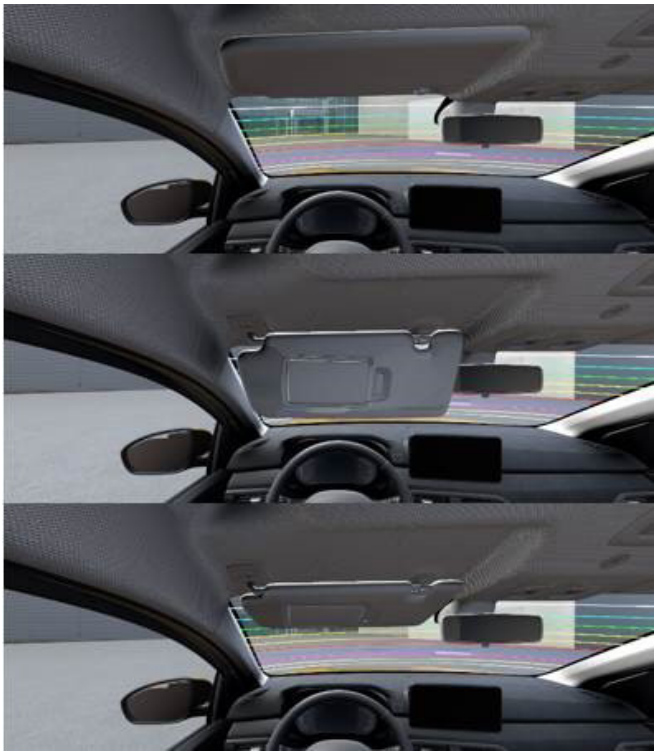

Fig. 5 Driver's view – H95

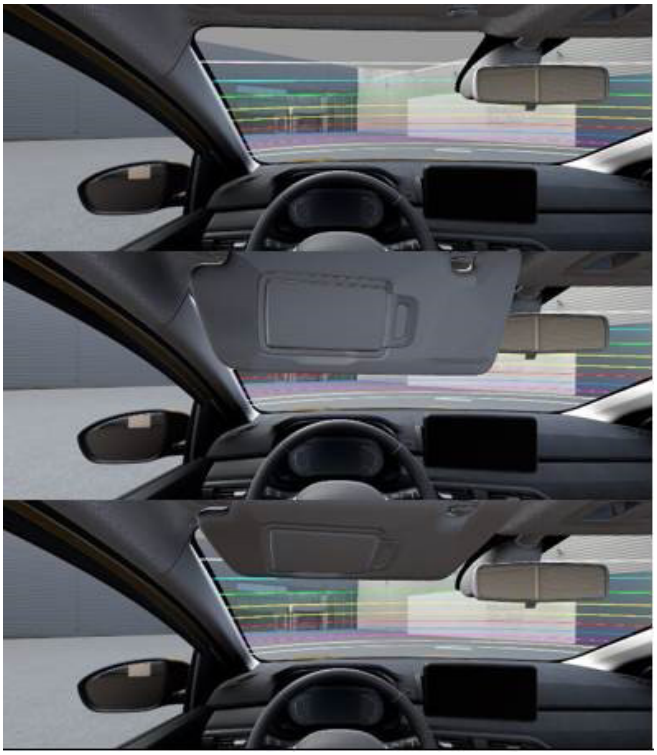

Fig. 6. Driver's view – Ref50

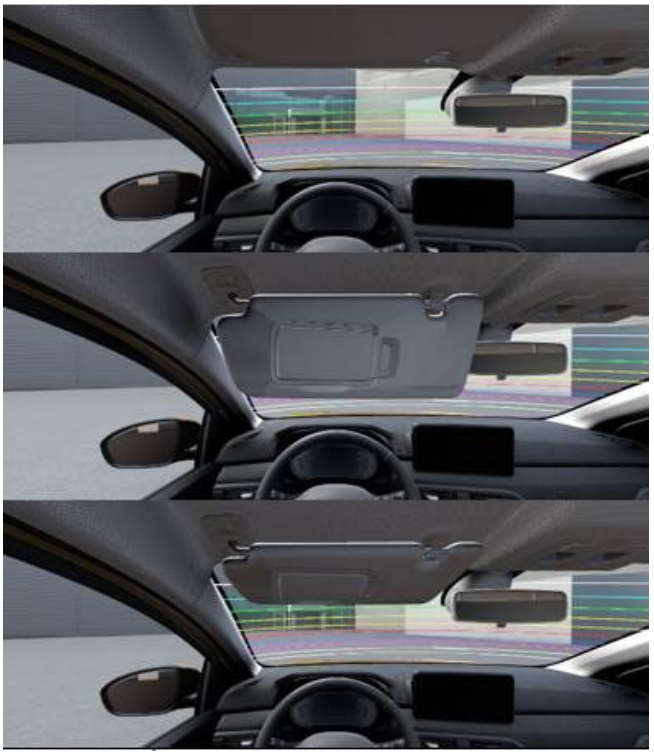

Fig. 7. Driver's view – R-H

will be represented by red color and is positioned in the middle.
For the beginning the extreme classes F5 and H95 were analyzed.
The F5 class represents 5% of European women. Here, all the visibility cases are in great parameters (Figure 4).
The H95 class addresses tall people. The testing dummy is 188cm tall. For that reason, the driving seat is in the extreme back position. At 120 degrees position of the sun visor, all the visual field is obturated (Figure 5). When is fully opened (170 degree) the dimension and position of the sun visor is at the limit of the comfort zone – red line.

Thus, is possible to create some safety problems when the motor vehicle runs at high speeds and the driver must open the sun visor.
Opening the sun visor, in the Ref50 class, where 90% of customers are, the lower edge is almost over the limit zone (Figure 6). When it is fully opened is above the comfort zone.
For 75% of the Europeans, meaning the R-H class, the 120 degrees position creates an unsafe zone by passing two lines the limit (Figure 7).

3.2 Objective results

To see the real benefits of the Digital mock-up with the CAVE, different

Fig. 8. The real driving seat used inside the CAVE

engineers participated to the tests. They were grouped in the three main classes small, tall, and medium.

They had to sit on a real driving seat (Figure 8) that was positioned inside the CAVE. To seat comfortable, they had to adjust the seat. After that they viewed the three positions of the sun visor (normal, 120 and 170 degrees). All the participants had to tell the lines that are visible, if the sunlight creates problems and if there are some remarks. Of the whole 10 lines, the 8th one was the green one that represents a good view. The limit of the view was the 4th one with the red color.

For the first class F5, the engineers said that the visual field is ok for all the positions of the sun visor, being able to see 8 lines.

A minor problem will appear if the sun is on the left and the direct sunlight passes through the screen pillar and the sun visor. In that case it will be easy to adjust the angle without affecting the view.

For the Ref50 class the view was within the normal limits, even if the sun visor was 120 degrees. In this position the driver had the tendency to bend forward even if the edge was one line above the red limit.

Engineers in the H95 class, that represents the tall ones, had an impediment at the crossing point of 120 degrees, because of the entire view obstruction. Only one line on the windscreen was visible. For the maximum angle of 170 degrees the view was within the normal limit, meaning that they could see the 8th line, the green one.

Using the subjective testing with the CAVE, no matter what the subject is, it is easy to perceive other problems. One of them was about the safety space above the head. During the objective analysis the engineers observed the problem and requested to modify the height or the shape of the roof before the physical prototype appeared.

At the end, all the participants were asked about their opinion about the CAVE. They said that they had a realistic perception, like being in a real vehicle.

4. CONCLUSIONS

The CAVE makes possible a visual analysis of the virtual prototypes. It helps perceiving things like the quality, the style, the architecture and not least the ergonomics of the model.

It is a necessary instrument in the interior vehicle design. The 3D analysis can determine the visibility of the driver on the steering wheel, dashboard legibility, command switches and the navigation screen. This way the designer can determine the command accessibility.

The possibility of studying the inside ergonomics helps in early detection of construction problems that affect the driver's or the passengers' comfort, all starting from the customers' suggestions of previous models.

It is easy to determine if the driver has a good front or back view. The frontal visual ellipse (SAE J 941 A) can be easily perceived, and the back view can be analyzed in the mirrors or directly by turning the head. All those views can be influenced by the shape, size, position of the interior components, like dashboard, seats, headrests etc. Not least the shape and size of the vehicle's body can influence the view but more than this the passengers' comfort. Every passenger has a comfort volume around the head that will influence the posture or even the safety in case a vehicle roll over, that could cause spinal problems.

Among other benefits, the CAVE makes possible a good collaboration between designers. Inside the room, where the CAVE is installed, can enter 10 persons. In the CAVE can enter 3 persons at the same time. Due to real time connectivity is possible to connect with others in different research locations around the world.

This way the repartition of the iterations along the motor vehicle life cycle will be higher in the beginning. Even if the number will be higher, the costs and time spent to produce the physical prototype will be lower. Reducing the number of iterations at the end of the design chain, in addition of reduced costs, the pollution will be lower. There will be less energy to use for the prototype production and testing.

Renault Techologie Roumanie accessed European funds of 800.000 Euros, investing 1.2 million Euros (Renault side). Right now, the Dacia Sandero, Logan and Jogger were models fully designed since the CAVE was implemented in Romania. The first model developed since 2019, the launch date of the CAVE, was Renault Arkana.

Just in the year 2022, Renault managed to save almost 2.8 million Euros with the CAVE and other digital simulations from the CAVE department. Normally, we see a digital model 1 year before industrialization and 2 years before it is launched so time and money saving are the top benefits of the CAVE, among the others.

ACKNOWLEDGEMENT

We greatly thank the industrial partner Renault Technologie Roumanie S.R.L. who made our application-oriented R&D work possible. Special thanks go to Mrs. Mariana VASILCA for her support and Mr. Constantin-Claudiu PIRVULESCU for his suggestions.

REFERENCES:

[1] A.M.K.P. Taylor, Science review of internal combustion engines, Energy Policy. 36 (2008) 4657–4667. doi:10.1016/j.enpol.2008.09.001.

[2] A. Clenci, R. Niculescu, On the compression ratio definition, in: SIAR (Ed.), 8th Int. Congr. ESFA, Organ. under FISITA Patronage, SIAR, Bucarest, 2009: pp. 49–55.

[3] J.H. Tuttle, Controlling Engine Load by Means of Late Intake-Valve Closing, SAE Tech. Pap. 800794. (1980). doi:10.4271/800794.

[4] J.M. Mallikarjuna, V. Ganesan, Optimization of inlet valve closure timing and clearance volume of a SI engine for better performance at part loads - A numerical and experimental approach, Indian J. Eng. Mater. Sci. 13 (2006) 307–321.

[5] O.A. Kutlar, H. Arslan, A.T. Calik, Methods to improve efficiency of four stroke, spark ignition engines at part load, Energy Convers. Manag. 46 (2005) 3202–3220. doi:10.1016/j.enconman.2005.03.008.

[6] B.R. de S. Ribeiro, Thermodynamic optimisation of spark ignition engines under part load conditions, Ph.D. Thesis. (2006).

[7] B. Ribeiro, J. Martins, Direct comparison of an engine working under Otto , Miller and Diesel cycles : Thermodynamic analysis and real engine performance, SAE Tech. Pap. (2007) 2007-01–0261. doi:10.4271/2007-01-0261.

[8] K. Stricker, L. Kocher, E. Koeberlein, D. Van Alstine, G.M. Shaver, Estimation of effective compression ratio for engines utilizing flexible intake valve actuation, Proc. Inst. Mech. Eng. Part D J. Automob. Eng. 226 (2012) 1001–1015. doi:10.1177/0954407012438024.

[9] D. Gruden, H. Richter, Torque characteristics and fuel efficiency of various gasoline engine concepts, SAE Tech. Pap. (1984). doi:10.4271/841284.

[10] F. Schäfer, R. van Basshuysen, Reduced Emissions and Fuel Consumption in Automobile Engines, Springer-Verlag Wien, 1995. doi:10.1007/978-3-7091-3806-9.

[11] J.B. Heywood, Internal Combustion Engine Fundamentals, 1988. doi:10987654.

[12] K. Stricker, L. Kocher, D. Van Alstine, G.M. Shaver, Input observer convergence and robustness: Application to compression ratio estimation, Control Eng. Pract. 21 (2013) 565–582. doi:10.1016/j.conengprac.2012.11.009.

[13] M. Klein, L. Eriksson, J. Åslund, Compression ratio estimation based on cylinder pressure data, Control Eng. Pract. 14 (2006) 197–211. doi:10.1016/j.conengprac.2005.03.022.

[14] A. Clenci, F. Ivan, R. Racota, Higher Expansion or Higher Compression at S.I.E.?, in: SIAR (Ed.), 7th Int. Conf. ESFA, Organ. under FISITA Patronage, SIAR, Bucharest, 2003.

[15] A. Clenci, P. Podevin, G. Descombes, Etude thermodynamique de la détente prolongée, in: SFT (Ed.), Colloq. Francoph. Sur l'Energie, Environnement, Econ. Thermodyn. COFRET'08, Nantes, 2008: pp. 11–13.

[16] P. Podevin, A. Clenci, Moteurs à taux de compression variable, in: Tech. l'Ingenieur, T.I., Techniques de l'Ingénieur, 2008: pp. 0–21.

[17] A. Biziiac, Cercetări privind ameliorarea performanțelor energetice ale unui motor cu aprindere prin scânteie prin realizarea variației înălțimii de ridicare a supapelor de admisie, Doctoral thesis, University of Pitesti, 2011.

CHALLENGE KART LOW COST 2023

UNIVERSITY OF PITEŞTI, „TITI AUR" ACADEMY, 11TH EDITION

UNIVERSITATEA DIN PITEŞTI, ACADEMIA „TITI AUR", EDIȚIA A 11-A

Zilele de 16 și 17 mai 2023 au marcat desfășurarea celei de-a 11-a ediții a concursului studențesc Challenge Kart Low Cost 2023, organizat de Universitatea din Pitești și Academia Titi Aur sub patronajul Societății Inginerilor de Automobile din România. Concursul studențesc internațional Kart Low Cost este o tradiție pentru studenții din domeniul ingineriei autovehiculelor și trebuie menționat faptul că acest lucru a fost posibil grație celor 16 ani de bună colaborare dintre Institutul Superior de Automobile și Transporturi (ISAT) din Nevers și Universitatea din Pitești.

Anul acesta, celor două universități deja menționate li s-au alăturat Universitatea Politehnica din București și Universitatea din Oradea, astfel că studenții au prezentat în total 4 proiecte dedicate propulsiei termice și 2 propulsiei electrice. Echipele participante au dezvoltat proiectele respectând regulamentul concursului în ceea ce privește concepția, fabricarea și testarea karturilor. Nu trebuie uitat faptul că proiectul este denumit Kart Low Cost pentru ca participanții să demonstreze că prin eforturi susținute pot dezvolta proiecte inginerești cu resurse financiare limitate (sub 2000 €, pentru kartul cu motor termic și sub 3000 € pentru cel electric), a căror validare se face rulând pe circuite sportive specifice.

În data de 16 mai, la Universitatea din Pitești au fost prezentate proiectele inginerești în fața unui juriu mixt, compus din membrii celor 4 universități. Studenții au prezentat în limba engleză aspecte ce țin de partea tehnică a concepției și fabricării karturilor, de design-ul acestora și, nu în ultimul rând, de justificare a încadrării în bugetul alocat.

În cea de-a doua zi a concursului, 17 mai, la Academia Titi Aur s-au derulat probele sportive, și anume: calificări, sprint, anduranță, accelerație 250m și slalom, unde studenții au demonstrat abilități spectaculoase de conducere a karturilor, dar și de rezolvare a problemelor tehnice ce au survenit pe parcursul probelor.

Am ajuns și la prezentarea câștigătorilor. Podiumul a fost ocupat de următoarele echipe:

- propulsia termică:
  - locul I - ISAT Nevers,
  - locul II - Universitatea din Pitești,
  - locul III - Universitatea din Oradea,
- propulsia electrică:
  - locul I - Universitatea din Pitești.

Echipele studențești au demonstrat că prin acțiuni susținute conduse pe parcursul a 6 luni de muncă se poate dezvolta un kart "low cost" care să ruleze cu succes pe un circuit specific sportiv.

Desfășurarea corespunzătoare a competiției KLC 2023 a fost posibilă ca și ca urmare a suportului oferit de Ministerul Educației, Academia Titi Aur, Dolotrans DTO Pitești, Proeco Gas Systems Pitești, Leoni, Mobilift, Văru' Nicu Motor Sport, Road Runner Racing Team.

Felicitări participanților și .... „à la prochaine à Nevers" !!!

Responsabili KLC România:
Ș.l. dr. ing. **Cătălin Zaharia** – Universitatea din Pitești
Prof. univ. dr. ing. **Adrian Clenci** – Universitatea din Pitești

IN MEMORIAM
PROF. UNIV. DR. ING. EUGEN MIHAI NEGRUŞ

A trecut aproape un an de când ne-a părăsit unul dintre membrii marcanți ai Societății Inginerilor de Automobile din România (SIAR), domnul prof. univ. dr. ing. Eugen-Mihai Negruș. Președinte fondator al SIAR din anul 1990, se poate spune că a fost motorul care a pornit activitatea SIAR între anii 1990-1993, iar apoi, între anii 1997-2012, perioadă în care a fost reales președinte SIAR, a fost factorul principal care a propulsat această societate, militând în special pentru recunoașterea SIAR la nivel internațional prin parteneriate cu alte societăți similare, precum FISITA, SAE, SIA și grupul european EAEC. Ca o recunoaștere a meritelor deosebite ale activității susținute în SIAR, a fost desemnat președinte de onoare al SIAR.

Principala activitate desfășurată de-a lungul a 62 de ani a fost legată de Departamentul Autovehicule Rutiere din Facultatea de Transporturi, Universitatea POLITEHNICA din București.

Am avut norocul să îl cunosc pe domnul profesor Eugen-Mihai Negruș, atât în perioada studenției când a fost unul dintre cei mai apreciați profesori, dar și ca unul dintre cei mai buni colegi din Departamentul Autovehicule Rutiere.

Ca fost student, am cele mai frumoase amintiri legate de cursurile domnului profesor Eugen-Mihai Negruș. Avea o bună comunicare cu studenții și știa să ne transfere toate informațiile necesare în formarea noastră. Avea grijă ca la curs să ne transmită și ultimele noutăți din domeniu, aducându-ne astfel un plus de cunoastere, mai ales că și disciplina studiată era pentru noi, studenții, foarte interesantă, *Cercetarea experimentală a autovehiculelor*. Domnul Negruș era în primul rând, om și apoi profesor. De aceea, deseori era un sprijin pentru studenții cu probleme. Universitatea POLITEHNICA din București este o instituție de marcă din România care a format ingineri de înaltă performanță profesională, care ne reprezintă cu mândrie atât la noi în țară cât și în afara granițelor. Se poate spune că domnul profesor Eugen-Mihai Negruș a fost unul dintre formatorii a zeci de generații de ingineri de autovehicule rutiere, cărora le-a îndrumat primii pași în activitate profesională. Puțini sunt acei absolvenți ai facultății noastre care nu-și mai amintesc cu aceeasi plăcere și recunoștință de cine era de fapt, domnul profesor Eugen-Mihai Negruș: un model de om si dascal.

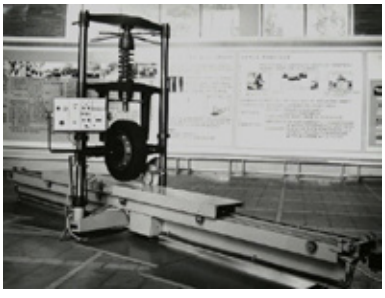

Timp de 34 de ani am fost și coleg cu domnul profesor Eugen-Mihai Negruș în Departamentul Autovehicule Rutiere din UPB, care a știut să își pună amprenta în formarea tinerelor cadre didactice, să orienteze și să dezvolte activitatea didactică și științifică a departamentului, reușind să își impună ideile într-un mod jovial.

Pentru cei care nu l-au cunoscut, așa ca noi, foștii colegi, vreau să amintesc câteva repere ale activității domnul profesor Eugen-Mihai Negruș.

Este bine de știut că s-a născut la 14.10.1937, la Bălți (în prezent în Republica Moldova). A absolvit Facultatea de Transporturi, Institutul Politehnic din București, în 1960, an în care a fost înființată și Catedra Autovehicule. Astfel se poate spune că domnul profesor Negruș și-a început activitatea profesională ca tânăr asistent universitar odată cu înființarea Departamentului de Autovehicule Rutiere, a parcurs toate etapele dezvoltării carierei sale didactice și în cadrul căruia a activat ca profesor universitar emerit până în ultimele clipe ale vieții.

Urmare a activității didactice și de cercetare întreprinse, a obținut titlul de doctor inginer în anul 1974, a devenit profesor universitar în 1990 și conducător de doctorat în anul 1991, activitate susținută aproape 30 de ani, în care a reușit să "rodească" câteva zeci de doctor ingineri. De mai multe ori îmi spunea că studiile și rezultatele cercetărilor efectuate nu e suficient doar să le comunicăm ci trebuie să le facem să rodească, să le fructificăm.

Din punct de vedere al activității administrative, domnul profesor Eugen-Mihai Negruș a fost și prodecan dar și apoi Decan al Facultății de Transporturi în perioada 1989-1996, iar între anii 2000-2007, membru în Comisia de atestare a titlurilor științifice a Ministerului Educației și Cercetării.

Activitatea didactică s-a concentrat în special pe Cercetarea experimentală și încercarea autovehiculelor, disciplină pentru care a înființat

laboratoare dezvoltate și pentru activități de cercetare. A fost autor a patru manuale universitare, două îndrumare de laborator, cinci manuale pentru licee de profil și două brevete de invenții înregistrate la OSIM.

Din anul 1977 a inițiat și dezvoltat o direcție nouă de cercetare științifică multidisciplinară, în tara noastră, în domeniul interacțiunii pneu-drum, realizând "Laboratorul mobil pentru simularea distribuției forțelor specifice în pata de contact în condiții de drum" și "Standul pentru măsurarea distribuției forțelor specifice în pata de contact pneu-cale de rulare, la viteze mici de rulare". A fost director de subprogram privind elaborarea unui material suport, pentru Proiectul Phare European Tyre School, Nokia – Finlanda. Acest domeniu de cercetare a constituit obiectul unei colaborări de durată cu industria românească și cu Universitatea Tehnică din Darmstadt, Germania.

Rezultatele activității de cercetare au constituit subiectul a peste 90 de comunicări științifice cu autor unic sau coautor, prezentate la congrese și conferințe internaționale și naționale, precum și seminarii științifice, dintre care trebuie menționate: Congresele monsiale SAE-Detroit 1998, 2002, 2003, FISITA1998 Paris, FISTA2000 Seoul, Conferințe EAEC1999 și 2005, dar, bineînțeles, și la toate congresele organizate de SIAR (ESFA București, CONAT Brașov, CAR Pitești, AMMA Cluj-Napoca) la care era nelipsit.

Intrucât știa ca industria de autovehicule românească și inginerii noștri au nevoie și de informații și schimburi de experiență cu specialiști din domeniul autovehiculelor din alte țării, în calitate de președinte al SIAR, a reușit să creeze punți de legătură solide cu alte societăți profesionale, așa cum am mai arătat, prin diferite funcții pe care le-a obținut, precum: membru din 1994 al SAE International; membru în Consiliul de conducere al FISITA și din Comitetul pentru educație continuă în ingineria de automobile; în perioada 1997-2005, membru în comitetul de coordonare al grupului european EAEC; ales în "Section Activities Board" al SAE International; nominalizat ca membru în "Education Comitee" al SAE International în 2004.

Activitatea excepțională pe care domnul profesor Eugen-Mihai Negruș a avut-o de-a lungul vieții a fost încununată cu distincții și decorații, dintre care trebuie să amintesc: Ordinul Național "Pentru merit", în gradul de Cavaler, conferit prin Decretul Prezidențial nr. 967/2002; Distincții acordate de SAE, USA, pentru activitate depusă cu dedicație (1998, 1999, 2000, 2003); "Profesor onorific", acordat de Senatul Universității Transilvania din Brașov; "Profesor emerit", acordat de Senatul Universității POLITEHNICA din București.

Putem spune fără reținere că domnul profesor Eugen-Mihai Negruș va rămâne în amintirea noastră un model de dascăl pentru zeci de generații de ingineri, un coleg neprețuit și un specialist în domeniul ingineriei autovehiculelor care, prin tot ce a făcut, a lăsat un gol încă necompletat.

Conf. univ. dr. ing. **Mihail-Daniel IOZSA**
Vicepreședinte SIAR
Directorul Departamentului de Autovehicule Rutiere
Universitatea POLITEHNICA din București

SISTEME DE ACȚIONARE HIDRAULICĂ

Autori (*Authors*): **Nicușor BAROIU, Georgiana-Alexandra MOROȘANU**
Editura (*Published by*): ACADEMICA
Anul apariţiei (*Published*): 2022
ISBN: 978-606-606-011-0

Această lucrare este concepută spre a fi suport de curs pentru disciplina *Acționări hidraulice* în cadrul programelor de studii universitare *Tehnologia Construcțiilor de Mașini, Inginerie Economică Industrială, Inginerie Mecanică, Sisteme și Echipamente Termice, Autovehicule Rutiere, Electromecanică, Inginerie Electrică și Calculatoare, Electronică de Putere și Acționări Electrice etc*. din cadrul Universității „Dunărea de Jos" din Galați . Pe lângă noțiunile consacrate, sunt introduse și elementele de noutate, conform tendințelor actuale din domeniul specificat. Lucrarea este structurată pe șapte părți principale, permițând prezentarea informațiilor într-o succesiune logică, adaptată necesității de a înțelege și opera astfel de sisteme de acționare.
Primul capitol oferă o introducere în domeniul sistemelor de acționare hidraulică, prezentând structura acestor sisteme, avantajele și dezavantajele utilizării lor și noțiunile teoretice, din fizică și mecanica fluidelor, care stau la baza funcționării sistemelor hidraulice.
În cel de al doilea capitol sunt prezentate elementele primare din structura sistemelor hidraulice și anume pompele hidraulice. Este realizată o clasificare a tipurilor de pompe, în funcție de debit și construcție, iar în finalul capitolului sunt prezentate instalațiile utilizate pentru testarea pompelor.
Capitolul trei este destinat elementelor secundare din componența sistemelor hidraulice, motoarele hidraulice. Se realizează o clasificare a acestor motoare, sunt prezentate elementele constructive ale acestora și, în continuarea capitolului, sunt analizate diferitele tipuri de motoare hidraulice.
În capitolul al patrulea autorii se concentrează pe elementele de comandă și reglare. Sunt analizate, din punct de vedere constructiv și funcțional, distribuitoarele hidraulice cu bile, distribuitoarele rotative, cele cu sertar și distribuitoarele hidraulice pilotate.
Al cincilea capitol prezintă elementele de comandă, control și reglare. Sunt prezentate supapele hidraulice simple și duble, supapele de limitare a presiunii, supapele de reducere a presiunii și cele de cuplare și decuplare. La finalul capitolului sunt prezentate instalațiile de testare a supapelor.
Capitolul șase este rezervat elementelor de reglare și control a debitului, respectiv elemente de tip drosel, rezistențe hidraulice și instalații de testare a acestora.
În final, capitolul șapte prezintă elementele hidraulice auxiliare precum: rezervoare, conducte și sisteme de cuplare, filtre, acumulatoare hidrostatice și elemente de etanșare.

INTRODUCERE ÎN SISTEMELE AUTOVEHICULELOR

Autori (*Authors*): **Călin ICLODEAN**
Editura (*Published by*): RISOPRINT Cluj-Napoca
Anul apariţiei (*Published*): 2023
ISBN: 978-973-53-2991-4

Această carte se adresează nu doar inginerilor absolvenți ai specializărilor de autovehicule și transporturi, se adresează și inginerilor care provin din alte domenii ide studii: calculatoare, electronică, mecanică, absolvenților care provin de la facultățile de fizică, chimie, matematică, științele mediului și alte specializări. Toți cei care folosesc această carte au oportunitatea de a-și dezvolta aptitudinile într-o abordare modernă și actuală a domeniului de inginerie a autovehiculelor.
Cartea este structurată pe zece capitole care tratează printr-o abordare multi și interdisciplinară noțiunile introductive în sistemele autovehiculelor de la descrierea *Embedded Systems* la metodologia de dezvoltare a unui „Virtual Model" pentru un autovehicul.
Capitolul 1 prezintă descrierea generală pentru *Embedded System* în general, respectiv pentru *Electronic Control Unit* în particular.
Capitolul 2 prezintă principalele unități de control care fac parte din *Powertrain and Transmission Domain*.
Capitolul 3 prezintă principalele unități de control care fac parte din *Chassis and Safety Domain*.
Capitolul 4 prezintă principalele unități de control care fac parte din *Body and Comfort Domain*.
Capitolul 5 prezintă principalele unități de control care fac parte din *Infotainment Domain*.
Capitolul 6 prezintă principalele unități de control care fac parte din *Telematics Domain*.
Capitolul 7 prezintă principalele rețele de comunicație utilizate în sectorul automobilelor atât din punct de vedere a arhitecturii constructive, cât și din punct de vedere a protocolului de comunicație.
Capitolul 8 prezintă *AUTOSAR*, o arhitectura software deschisă utilizată în proiectarea *Electronic Control Unit*.
Capitolul 9 prezintă metodologia de dezvoltare a *Virtual Models* utilizate în simulările computerizate.
Capitolul 10 prezintă *V-Cycle* sau *diagrama V* care descrie ciclul de proiectare-dezvoltare-implementare pornind de la un model virtual la un model real de sistem/ autovehicul.
Volumul – cuprinzând 706 pagini, cu o bibliografie cuprinzătoare detaliată la fiecare capitol - poate fi lecturat online pe pagina web: https://www.calin.co.ro/

Lucrările prezentate fac parte din fondul bibliografic al Centrului de documentare al SIAR.

REGISTRUL AUTO ROMÂN

www.autotestmagazin.ro
www.facebook.com/RegistrulAuto
www.facebook.com/autotestmagazin

Programări
la numărul
021/9672
și pe
www.rarom.ro